Vibroacoustic subtractive modeling using a reverse condensed transfer function approach

F. Dumortier, Laurent Maxit, V. Meyer

Vibroacoustic subtractive modeling using a reverse condensed transfer function approach

F. Dumortier[a,b,*], L. Maxit[a], V. Meyer[b]

[a] *INSA Lyon, Laboratoire Vibrations Acoustique, 25 bis av. Jean Capelle, 69621 Villeurbanne Cedex, France*
[b] *Naval Group Research, 199 av. Pierre-Gilles de Gennes, 83190 Ollioules, France*

Abstract

Substructuring methods are a very common and efficient way to solve complex vibroacoustic problems. The Condensed Transfer Function (CTF) approach is a substructuring method based on the concept of subsystem condensed transfer functions (corresponding to admittances or impedances) that allows assembling acoustical or mechanical subsystems coupled along lines or surfaces. For certain practical applications, it may be more efficient to subtract or to decouple a subsystem to a global system rather than assembling different subsystems. In this paper, a reverse formulation of the CTF method is proposed. This formulation allows us to predict the behavior of a subsystem that is part of a larger system, from the knowledge of the condensed transfer functions (CTFs) of the global system and of the residual subsystem that must be removed. For purposes of validation, the scattering problem of a rigid sphere in an infinite water domain impacted by an acoustic plane wave is considered. Comparisons with theoretical calculations are used to validate the formulation proposed and permit studying its accuracy for two types of condensation functions defining the CTFs.

Keywords:
Numerical modeling, Substructuring method, Decoupling method, Subtractive modeling, Surface impedance.

* Corresponding author
Email address: florent.dumortier@insa-lyon.fr (F. Dumortier)

Nomenclature

a	Radius of the sphere, defined in table 1
c_0	Sound speed, defined in table 1
d	Size of the patch, appearing in Eq. (31)
$H_{p/Q}\,(M, M')$	Transfer function between the volume velocity flow of a monopole source at point M' and the pressure at point M, defined in section 3.2
$h_n^{(1)}$	Spherical Hankel function of the first kind, appearing in Eq. (A.1a)
$h_n^{(2)}$	Spherical Hankel function of the second kind, appearing in Eq. (A.1a)
$\boldsymbol{I}$	Identity matrix, appearing in Eq. (16)
i	Imaginary unit, appearing in Eq. (32)
j_n	Spherical Bessel function of the first kind, appearing in Eq. (34)
k_0	Wavenumber, appearing in Eq. (32)
L_p	Sound pressure level, defined in Eq. (37)
N	Number of condensation functions, defined in section 4.2.1
N_L	Maximal degree of the associated Legendre polynomial, defined in section 4.2.1
$p_\alpha(\boldsymbol{x})$	Pressure at the junction of subsystem α, defined in Eq. (1)
P_α^i	Condensed pressure at the junction of subsystem α associated with the condensation function φ^i, appearing in Eq. (1)
p_0	Reference pressure, defined in section 4.4.2
$P_n^m(\cos\theta)$	Associated Legendre polynomial, appearing in Eq. (25)
$\tilde{\boldsymbol{P}}_{\boldsymbol{\alpha}}^{\boldsymbol{M}}$	Condensed blocked pressure vector of subsystem α induced by a unit volume velocity located at point M, defined in section 3.2

$\boldsymbol{P}_{\boldsymbol{\alpha}}^{\boldsymbol{\delta}}$ Condensed pressure vector of subsystem α with a prescribed velocity jump, appearing in Eq. (19)

P_i Incident pressure of the plane wave, appearing in Eq. (33)

p_i^M Incident pressure of the spherical source at point M, appearing in Eq. (B.1)

$P_n(\cos\theta)$ Legendre polynomial, appearing in Eq. (34)

$\boldsymbol{P}_{\boldsymbol{\alpha}}$ Condensed pressure vector of subsystem α, defined in section 2

$\boldsymbol{P}_{\boldsymbol{\alpha}}^{\boldsymbol{M}}$ Condensed pressure vector of subsystem α induced by a unit volume velocity located at point M, defined in section 3.2

$p_{s\infty}$ Scattered pressure by the rigid sphere, defined in Eq. (35)

$\tilde{\tilde{p}}_\alpha$ Blocked pressure at the junction of uncoupled subsystem α, defined in section 2

$\tilde{P}_\alpha^i$ Condensed blocked pressure at the junction of subsystem α associated with the condensation function φ^i, defined in Eq. (4)

$\tilde{\boldsymbol{P}}_{\boldsymbol{\alpha}}$ Condensed blocked pressure vector of subsystem α, defined in section 2

$Q(M)$ Volume velocity flow of a monopole source at point M, defined in section 3.2

R Radial distance to origin, shown on figure 4

$u_\alpha(\boldsymbol{x})$ Normal velocity at the junction of subsystem α, defined in Eq. (1)

U_α^i Condensed normal velocity at the junction of subsystem α associated with the condensation function φ^i, appearing in Eq. (1)

δU_{1+2}^i Condensed normal velocity jump at the junction of subsystem $1+2$ associated with the condensation function φ^i, appearing in Eq. (17)

$\boldsymbol{\delta U}$ Condensed normal velocity jump vector, defined in Eq. (18)

$\boldsymbol{U}_{\boldsymbol{\alpha}}^{\boldsymbol{\delta}}$ Condensed normal velocity vector of subsystem α with a prescribed velocity jump, appearing in Eq. (19)

$\boldsymbol{U}_{\boldsymbol{\alpha}}$ Condensed normal velocity vector of subsystem α, defined in section 2

y_n Spherical Bessel function of the second kind, appearing in Eq. (A.1b)

$\boldsymbol{Z_\alpha}$ Condensed impedance matrix of subsystem α, defined in section 2

$Z^i_\alpha(M_\alpha)$ Point condensed impedance vector of subsystem α at point M_α associated with the condensation function φ^i, defined in section 2

$\boldsymbol{Z_\alpha}(M_\alpha)$ Point condensed impedance vector of subsystem α at point M_α, defined in section 2

Z^{ij}_α Condensed transfer function of subsystem α between φ^i and φ^j, defined in Eq. (2)

δ_{ij} Kronecker symbol, appearing in Eq. (28)

$\varepsilon^i_{n,m}$ Evaluation factor associated with the condensation function φ^i, defined in Eq. (A.10)

η Loss factor, defined in table 1

κ_m Even factor, defined in Eq. (B.3)

λ Wavelength, appearing in Eq. (30)

φ^i Condensation function, defined in section 2

ϕ Azimuthal angle, shown on figure 4

$\psi_{m,n}$ Spherical harmonics, defined in Eq. (25)

ρ Density, defined in table 1

θ Polar angle, shown on figure 4

ω Angular frequency, appearing in section 4.4.1

Ω Surface junction between the subsystems, defined in figure 2

Ω_i Surface of the patch, defined in section 4.2.2

1. Introduction

Substructuring methods in vibroacoustics have been widely investigated in recent decades to overcome the computational limitations of numerical methods. In particular, substructuring methods based on admittance and impedance concepts are a powerful tool for studying the vibroacoustic behavior of complex structures that can be partitioned into several substructures. Initially derived from electrical concepts by Firestone [1], they were then developed by Rubin [2] and O'Hara [3] and consist in the coupling of subsystems for which the characteristics are determined by different means (analytically, numerically or experimentally). Petersson and Plunt [4, 5] introduced the concept of effective mobilities for multi-point coupled structures to determine the sound power transmitted to a structure. The admittance method was then extended to structural-acoustic systems with weak coupling by Kim and Brennan [6].

Later on, Ouisse *et al.* [7] developed the Patch Transfer Function (PTF) method to couple subsystems along surfaces. The method is adapted for linear acoustics and linear vibro-acoustics problems. The coupling surfaces between the subsystems can either appear at a junction between a vibrating structure and an acoustic domain, or between two acoustic domains. The first step of the method consists in dividing the coupling surfaces into elementary surfaces called patches using a wavelength-based criterion while in the second step each subsystem is studied independently to build a set of transfer functions defined by using mean values on the patches; hence the term Patch Transfer Functions. For structural subsystems, the PTFs correspond to admittances (displacement over force) whereas for subsystems consisting of an acoustic domain, they correspond to impedances (pressure over velocity). Then, the PTFs are assembled by using the superposition principle for the linear passive system along with the continuity relations, leading to the fast resolution of the coupled problem. This method has shown to be of great interest for estimating the noise radiated outside a vehicle [7, 8], predicting transmission loss through double panels filled with porogranular materials [9, 10], modeling the effect of micro-perforated panels in a complex vibroacoustic environment [11, 12] and for acoustic silencing in a flow duct [13]. The PTF method was also used in inverse methods to identify and characterize vibrating sources [14–16]

The convergence of the approach was improved by Aucejo *et al.* [17], particularly for strong coupling, by introducing residual mode shapes. Maxit *et al.* [18] proposed a way to reduce the number of patches by partitioning the subsystems outside the acoustic near field of the structures, and applied the method to sound transmission through ballast compartments in a submarine. As

a generalization of the PTF method to vibroacoustic partitioning along lines or surfaces, Meyer *et al.* developed the Condensed Transfer Function (CTF) method [19]. The displacements and forces at the junctions of the subsystems are decomposed into a set of orthonormal functions called condensation functions. The unknowns of these decompositions are estimated using the condensed transfer functions (CTFs) defined for each uncoupled subsystem using a scalar product and the condensation functions. As for the PTFs, the CTFs are assembled by using the superposition principle for the linear passive system to ensure displacement continuity and force equilibrium at the junctions. The PTF approach can be seen as a particular case of the CTF approach, where the condensation functions correspond to 2D gate functions. Meyer *et al.* [19] studied the influence of three different kinds of condensation function (gate functions, complex exponential functions and Chebyshev polynomials) on the numerical convergence of the method. Criteria of convergence were defined for these different types of condensation functions and it was shown that they present similar performances. The approach was applied to study the acoustic radiation of stiffened cylindrical shells with non-axisymmetric internal frames [20]. Two types of condensation function were used: complex exponentials were used for coupling between cylindrical shell and ring stiffeners whereas gate functions were used for coupling with non-axisymmetric internal frames. Later, an optimal piecewise convergence criterion was established by Hu *et al.* [21] when considering complex exponential functions as condensation functions to couple plate-cavity systems in the mid-frequency range. The criterion was also applied to strong coupling modeling before being validated experimentally [22].

Although the coupling of subsystems has been widely investigated, it can sometimes be useful to decouple subsystems. For instance this can be illustrated by the case shown in figure 1 in which the effect of a void cavity (i.e. a default) in a multilayered cylinder is modeled. Analytical models of multilayered cylinders exist in the literature (see references [23–27]) but only numerical methods like FEM can be used to model a multilayered cylinder with a void cavity, leading to very considerable computation times. To tackle this issue, we aim at developing a subtractive method that could be used in this illustrative example to subtract from the analytical multilayered cylinder model a numerical model of the part of the multilayered cylinder corresponding to the geometry of the void cavity (see figure 1).

As far as the authors know, such a general subtractive approach has not yet been developed. Nonetheless, some authors have already proposed several developments of decoupling approaches

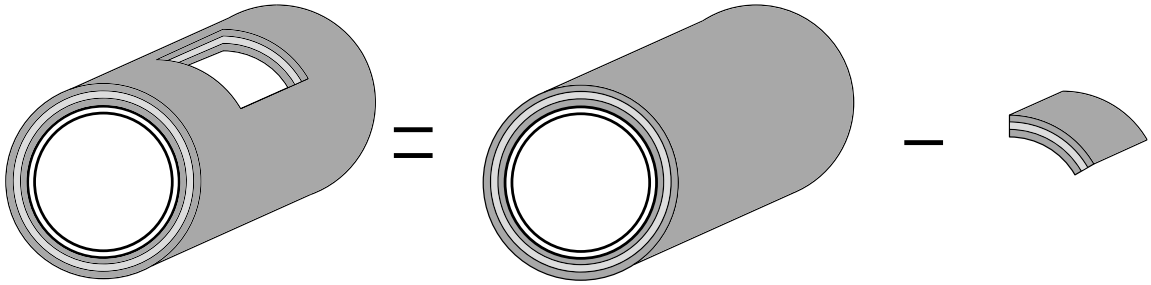

Figure 1: Subtractive modeling on a cylindrical shell with void.

to address particular cases. Indeed, Soedel and Soedel [28] proposed a reverse formulation of the receptance method, where the receptance is defined as the ratio of a deflection response at a point to a harmonic force or a moment input at a point, to remove a spring from an automobile suspension system. This approach using point receptances was extended to line receptances by Huang and Ting [29] to deduce the frequencies and mode shapes of an annular plate from the study of a circular plate and a smaller deducted circular plate. Several similar studies of the reverse receptance approach (RRA) were conducted [30, 31] and concluded that the efficiency of the method is directly linked to the size of the deducted subsystem (the void in figure 1), compared to the size of the initial system (the fully coated multilayered cylinder in figure 1). A higher ratio between the size of the deducted subsystem and the size of the initial system will lead to greater errors. In these previous studies, the reverse approaches were developed for specific dedicated cases. Moreover, they were generally focused on the estimation of the receptance of the decoupled subsystems and not on the prediction of the subsystem's response to external excitations. D'Ambrosio and Fregolent [32] also explored decoupling procedures by estimating the dynamic behavior, in terms of Frequency Response Functions (FRFs), from the knowledge of the FRFs of the larger system and the physical model of the second subsystem. This study highlighted ill-conditioning at the neighbourhood of certain natural frequencies of the known subsystems, leading to great sensitivity to measurement errors. To tackle this issue, the definition of the interface between the subsystems was extended by taking into account some internal DoFs of the residual subsystem in [33], or by using a dual formulation of the problem in [34]. This method has proved to be efficient in the updating of the FRF during machining removing, with predictions 20 times faster than full order finite element models in [35]. We can emphasize that the subsystems in these papers ([32–35]) are represented by discrete models (based on FRF), and the coupling interfaces are then generally reduced to points.

Furthermore, they focus on the vibratory aspect and are oriented for experimental applications. Compared to these studies, we propose in the present paper a formalism based on continuous, mechanical or acoustic, subsystems exhibiting continuous (lines or surfaces) coupling interfaces. The expected applications mainly concern numerical simulations in vibroacoustics.

The goal of the present paper is therefore to generalize this principle of reverse approach to more general cases than those studied in the past. This generalization is achieved thanks to the concept of CTFs which have shown their ability to deal with various situations. The reverse formulation of the CTF approach proposed in this paper is not limited to the evaluation of the CTFs of the decoupled subsystems, and can be applied to various problems, either vibratory, acoustical, or vibroacoustical. The developments are carried out to predict the response at any point of the decoupled subsystems excited by an external source. For the purposes of validation, the approach proposed is compared with a reference calculation on an academic test case consisting of the scattering of an acoustic plane wave by a rigid sphere in an infinite water medium. This test case has been chosen because it has been deeply studied in the past (see for instance in [36–38]) and constitutes a reference for the study of the acoustic scattering by naval structures. Moreover, in the future, it could be easily upgraded to study the scattering of spheres coated by a soft rubber material [39, 40]. This method could also be applied to the practical case illustrated on figure 1 consisting in the modeling of a multi-layered cylinder with a void cavity. Starting from an analytical model of the multilayered cylinder and the finite element model of the part to be subtracted (i.e. the part of the material constituting the multilayered coating), the reverse CTF method could be used to predict the behaviour of the multilayered cylinder with the void cavity. For the case of the scattering of a plane wave by a rigid sphere, the reverse CTF approach consists in subtracting a sphere of water (having the geometry of the rigid sphere) from the infinite water medium. The accuracy of the method is then studied with two types of condensation function. The paper is organized as follow:

- In Section 2, the principle of the direct CTF approach is recalled in the case of acoustic problems. Descriptions of the approach for the cases of vibroacoustic problems or purely mechanical problems can be found in the litterature [19, 21];
- The reversed CTF formulation is then proposed in Section 3. The principle is described in Section 3.1 whereas the different needed quantities to apply it are described in the following sub-sections;

- In Section 4, a numerical validation of the test case with the two types of condensation functions is proposed, before concluding in Section 5;
- The main text is completed by two appendices presenting the calculation of the CTFs and the condensed blocked pressures related to the test case of Section 4.

2. Principle of the direct CTF method for acoustic problems

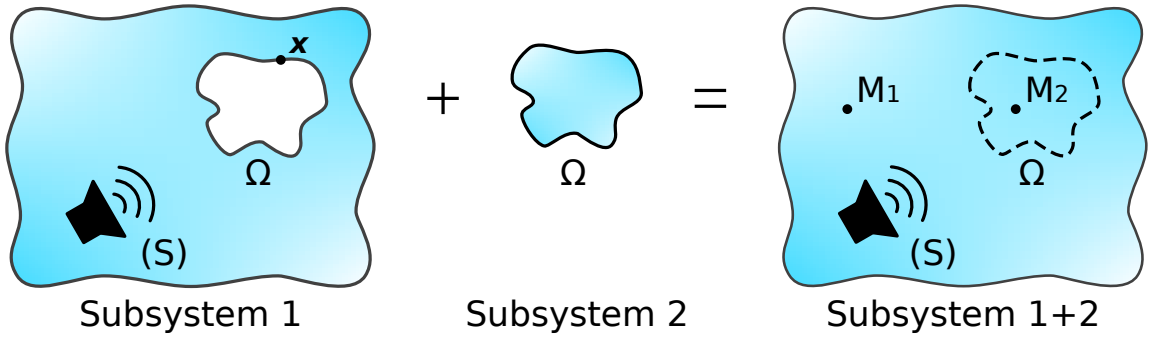

Figure 2: Principle of the direct CTF method.

In this section, the principles of the CTF approach for an acoustic problem are recalled (see the references of Meyer [19] and Hu [21] for details and for vibroacoustic and mechanical problems). Let us consider two acoustical domains coupled along a surface Ω, where $\boldsymbol{x}$ is a point on Ω, and excited by an acoustic source (S) applied on subsystem 1, as shown in figure 2. The contacts are assumed to be perfect and without friction loss, and the responses are calculated in harmonic regime. A set of N orthonormal functions defined on Ω, called the condensation functions, is considered: $\{\varphi^i\}_{1\leqslant i\leqslant N}$. It is assumed that for each subsystem α, the pressures p_α and the normal velocities u_α (where the outer-pointing normal is defined as positive) at the junction can be approximated as a linear combination of the condensation functions:

$$p_\alpha(\boldsymbol{x}) \simeq \sum_{i=1}^{N} P_\alpha^i \varphi^i(\boldsymbol{x}) \quad \text{and} \quad u_\alpha(\boldsymbol{x}) \simeq \sum_{i=1}^{N} U_\alpha^i \varphi^i(\boldsymbol{x}) \quad \forall \boldsymbol{x} \in \Omega \tag{1}$$

where P_α^i and P_α^i are the unknowns. To estimate them, it is necessary to define for each uncoupled subsystem $\alpha \in \{1, 2\}$, the condensed transfer function between φ_i and φ_j by applying a prescribed velocity $u_\alpha = \varphi^j$ on Ω:

$$Z_\alpha^{ij} = \frac{\langle \bar{p}_\alpha, \varphi^i \rangle}{\langle u_\alpha, \varphi^j \rangle} = \langle \bar{p}_\alpha, \varphi^i \rangle \tag{2}$$

with $\bar{p}_\alpha$ the resulting pressure at the junction Ω when the subsystem is excited by $u_\alpha = \varphi^j$ and $\langle \bullet, \bullet \rangle$ the scalar product defined on the surface Ω by:

$$\langle f, g \rangle = \iint_\Omega f(\boldsymbol{x}) g^*(\boldsymbol{x}) \, \mathrm{d}\boldsymbol{x} \tag{3}$$

where * denotes the complex conjugate. Moreover, the condensed blocked pressure of each uncoupled subsystem α is defined by:

$$\tilde{P}_\alpha^i = \langle \tilde{\bar{p}}_\alpha, \varphi^i \rangle \tag{4}$$

where $\tilde{\bar{p}}_\alpha$ is the pressure at the junction of the uncoupled subsystem α when only external loading is applied. Assuming there is no external load applied on subsystem 2, $\tilde{P}_2^i = 0, \forall i \in [\![0, N]\!]$.

In the following, the condensed impedance matrix of subsystem α will be refered as $\boldsymbol{Z_\alpha}$, where the coefficient of the i^{th} row and j^{th} column corresponds to Z_α^{ij}. Similarly, $\boldsymbol{U_\alpha}$, $\boldsymbol{P_\alpha}$ and $\boldsymbol{\tilde{P}_\alpha}$ will denote the condensed velocity vector, the condensed pressure vector, and the condensed blocked pressure vector associated with subsystem α, respectively.

An external load (S) and a prescribed velocity u_1 on Ω are applied on subsystem 1, whereas only a prescribed velocity u_2 on Ω is applied on subsystem 2. In response to these prescribed velocities and the external load, the superposition principle for linear passive systems [20] gives us expressions relating to the condensed velocities and pressure vectors:

$$\begin{cases} \boldsymbol{P_1} = \boldsymbol{\tilde{P}_1} + \boldsymbol{Z_1 U_1} \\ \boldsymbol{P_2} = \boldsymbol{Z_2 U_2} \end{cases} \tag{5}$$

The velocity continuity and force equilibrium at the junction yields (taking into account the definition of the normals)

$$\begin{cases} p_1(\boldsymbol{x}) = p_2(\boldsymbol{x}) \\ u_1(\boldsymbol{x}) + u_2(\boldsymbol{x}) = 0 \end{cases}, \quad \forall \boldsymbol{x} \in \Omega \tag{6}$$

By injecting Eq. (1) in Eq. (6) and projecting the results on the condensation functions, one obtains:

$$\begin{cases} \boldsymbol{P_1} = \boldsymbol{P_2} \\ \boldsymbol{U_1} + \boldsymbol{U_2} = 0 \end{cases} \tag{7}$$

In the following, when the two subsystems are coupled, $\boldsymbol{P_{1+2}}$ denotes the condensed pressure vector whereas $\boldsymbol{U_{1+2}}$ denotes the condensed velocity vector. By convention, $\boldsymbol{U_{1+2}} = \boldsymbol{U_1} = -\boldsymbol{U_2}$ and $\boldsymbol{P_{1+2}} = \boldsymbol{P_1} = \boldsymbol{P_2}$. By combining Eq. (5) and Eq. (7), the coupling velocities $\boldsymbol{U_{1+2}}$ between the two subsystems can be deduced:

$$(\boldsymbol{Z_1} + \boldsymbol{Z_2})\,\boldsymbol{U_{1+2}} = -\tilde{\boldsymbol{P}}_{\boldsymbol{1}} \tag{8}$$

Once the coupling velocities have been calculated, the response at given points M_1 (in subsystem 1) and M_2 (in subsystem 2) can be deduced:

$$\begin{cases} p_{1+2}(M_1) = \tilde{p}_1(M_1) + \boldsymbol{Z_1}(M_1)\boldsymbol{U_{1+2}} & \text{(9a)} \\ p_{1+2}(M_2) = -\boldsymbol{Z_2}(M_2)\boldsymbol{U_{1+2}} & \text{(9b)} \end{cases}$$

$\boldsymbol{Z_\alpha}(M_\alpha)$ is the vector of the point condensed impedance and should be distinguished from the condensed impedance matrix $\boldsymbol{Z_\alpha}$. The i^{th} component of this vector, $Z^i_\alpha(M_\alpha)$, is defined as the pressure at point M_α when a normal velocity corresponding to the condensation function φ^i is prescribed on Ω.

3. Reverse CTF method

3.1. Principle

In this section, we develop the subtractive approach consisting in reversing the CTF approach. The behavior of the complete system 1+2 as well as that of subsystem 2 are assumed as known, and the aim of this development is to deduce the behavior of subsystem 1, as shown in figure 3. In Eq. (9a), $\tilde{p}_1(M_1)$ represents the pressure at point M_1 when subsystem 1 is uncoupled from subsystem 2. It is thus the quantity of interest for the present study. We can write:

$$\tilde{p}_1(M_1) = p_{1+2}(M_1) - \boldsymbol{Z_1}(M_1)\boldsymbol{U_{1+2}} \tag{10}$$

The coupling velocities $\boldsymbol{U_{1+2}}$ at the junction can be retrieved using Eq. (5) combined with the pressure continuity and velocity equilibrium of Eq. (7):

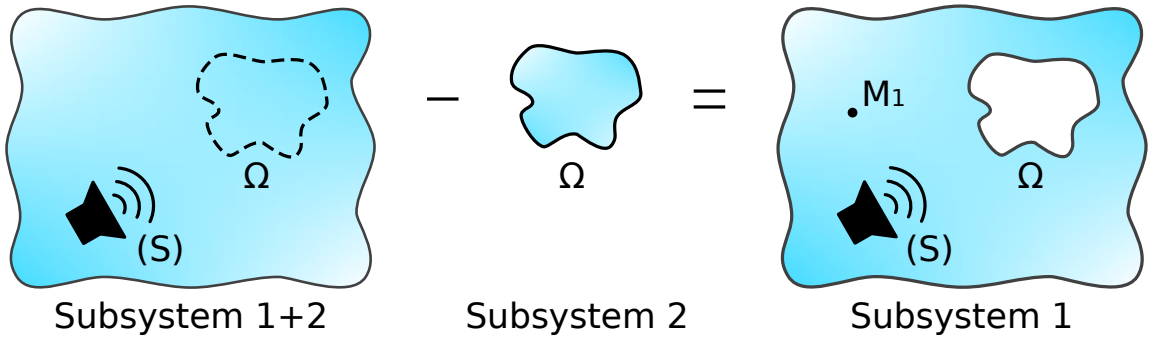

Figure 3: Principle of the reverse CTF method.

$$\boldsymbol{U_{1+2}} = -{\boldsymbol{Z_2}}^{-1}\boldsymbol{P_{1+2}} \tag{11}$$

Finally, the pressure at a given point M_1 of uncoupled subsystem 1 can be rewritten as:

$$\tilde{p}_1(M_1) = p_{1+2}(M_1) + \boldsymbol{Z_1}(M_1){\boldsymbol{Z_2}}^{-1}\boldsymbol{P_{1+2}} \tag{12}$$

As the behavior of subsystem 2 and of the global system 1+2 are assumed as known, $p_{1+2}(M_1)$, $\boldsymbol{Z_2}$ and $\boldsymbol{P_{1+2}}$ are therefore known quantities. In order to evaluate $\tilde{p}_1(M_1)$, the next subsections focus on determining $\boldsymbol{Z_1}(M_1)$ as well as $\boldsymbol{Z_1}$, the condensed impedance of subsystem 1.

3.2. Calculation of the point condensed impedance using a reciprocity principle

We now focus on the calculation of the impedance $\boldsymbol{Z_1}(M)$, with M being a given point located in the acoustic domain associated with subsystem 1. We recall that the i^{th} component of this vector, $Z_1^i(M)$, corresponds to the pressure at point M when a prescribed velocity corresponding to the condensation function φ^i is imposed on the coupling surface. It can be expressed as:

$$Z_1^i(M) = \iint_{\Omega} H_{p/Q}\left(M, M'\right)\varphi^i\left(M'\right)\mathrm{d}M' \tag{13}$$

where $H_{p/Q}\left(M, M'\right) = \frac{p(M)}{Q(M')}$ is the transfer function corresponding to the ratio between the pressure at point M and the volume velocity flow of the monopole source at point M'. In Eq. (13), $\varphi^i\left(M'\right)\mathrm{d}M'$ is the product between normal velocity $\varphi^i\left(M'\right)$ and elementary surface $\mathrm{d}M'$, and corresponds to a volume velocity flow. Hence, $H_{p/Q}\left(M, M'\right)\varphi^i\left(M'\right)\mathrm{d}M'$ represents the pressure at

point M induced by a monopole source of volume velocity $\varphi^i(M')\,\mathrm{d}M'$ and of elementary surface $\mathrm{d}M'$. The sum of these contributions over the surface Ω corresponds to the quantity $Z_1^i(M)$.

On the other hand, the reciprocity principle states that the response of a linear system to a time-harmonic disturbance that is applied at some point by an external agent is invariant with respect to exchange of points of input and observed response [41, 42]. In this case, it means that the pressure radiated at point M when it is excited by a monopole source of unit volume velocity at point M' equals the pressure radiated at point M' when it is excited by a monopole source of unit volume velocity at point M:

$$H_{p/Q}\left(M, M'\right) = H_{p/Q}\left(M', M\right) \tag{14}$$

Hence, Eq. (13) can be rewritten:

$$Z_1^i(M) = \iint_{\Omega} H_{p/Q}\left(M', M\right) \varphi^i\left(M'\right) \mathrm{d}M' \tag{15}$$

A new interpretation of $Z_1^i(M)$ can be given from Eq. (15). It corresponds to the pressure on the coupling surface projected on the condensation function φ^i, induced by a monopole source of unit volume velocity situated on point M. From this interpretation, $\boldsymbol{Z_1}(M)$ is therefore the vector of the blocked pressure on the coupling surface when the excitation is a monopole source of unit volume velocity: $\boldsymbol{Z_1}(M) = \tilde{\boldsymbol{P}}_{\boldsymbol{1}}^{\boldsymbol{M}}$. The exponent M is introduced in the notation to specify that the excitation considered is a unitary monopole located at point M.

This quantity, $\tilde{\boldsymbol{P}}_{\boldsymbol{1}}^{\boldsymbol{M}}$, can be estimated from the knowledge of the pressure induced by the monopole source on the global system 1+2. Let us assume that we know $\boldsymbol{P}_{\boldsymbol{1+2}}^{\boldsymbol{M}}$, the vector of the condensed pressure induced by the monopole source of unit volume velocity and located at the point M in the global system 1+2.

Eq. (5) and Eq. (7) related to the CTF approach can still be applied for the present case. From these equations, $\tilde{\boldsymbol{P}}_{\boldsymbol{1}}^{\boldsymbol{M}}$ can be expressed as

$$\tilde{\boldsymbol{P}}_{\boldsymbol{1}}^{\boldsymbol{M}} = \left(\boldsymbol{I} + \boldsymbol{Z_1}\boldsymbol{Z_2}^{-1}\right) \boldsymbol{P}_{\boldsymbol{1+2}}^{\boldsymbol{M}} \tag{16}$$

where $\boldsymbol{I}$ is the identity matrix.

At this stage, $\boldsymbol{Z_1}$ is still unknown. We will see in the next subsection how to estimate it from the condensed impedance matrix of subsystem 2, $\boldsymbol{Z_2}$, and of the global system, $\boldsymbol{Z_{1+2}}$.

3.3. Calculation of the condensed impedance of subsystem 1

Our aim in this subsection is to derive the condensed impedance matrix of subsystem 1, $\boldsymbol{Z_1}$, from those of subsystem 2 and the global system 1+2, respectively $\boldsymbol{Z_2}$ and $\boldsymbol{Z_{1+2}}$.

The condensed impedances of subsystems 1 and 2 were previously defined by Eq. (2). Let us now define the condensed transfer function of the global system 1+2 between φ^i and φ^j by applying a prescribed velocity jump at the junction Ω corresponding to the condensation function φ^j:

$$Z^{ij}_{1+2} = \frac{P^i_{1+2}}{\delta U^j_{1+2}} = \frac{\langle \bar{p}_{1+2}, \varphi^i \rangle}{\langle \varphi^j, \varphi^j \rangle} = \langle \bar{p}_{1+2}, \varphi^i \rangle \tag{17}$$

where $\bar{p}_{1+2}$ corresponds to the pressure at junction Ω resulting from the prescribed velocity jump, $\delta U^j_{1+2} = \varphi^j$.

The condensed velocity jump vector at the junction associated with the prescribed velocity jump corresponding to the condensation function φ^j is given by:

$$\boldsymbol{\delta U} = \begin{bmatrix} 0 \\ \vdots \\ 0 \\ 1 \\ 0 \\ \vdots \\ 0 \end{bmatrix}, \tag{18}$$

where the position of 1 corresponds to the j^{th} component. Eq. (5) and Eq. (7) related to the CTF approach can still be applied for this case, but as there is no external excitation in subsystem 1, and the prescribed velocity jump is applied at the junction, they are slightly modified:

$$\begin{cases} \boldsymbol{P^\delta_1} = \boldsymbol{Z_1 U^\delta_1} \\ \boldsymbol{P^\delta_2} = \boldsymbol{Z_2 U^\delta_2} \\ \boldsymbol{P^\delta_{1+2}} = \boldsymbol{P^\delta_1} = \boldsymbol{P^\delta_2} \\ \boldsymbol{\delta U} = \boldsymbol{U^\delta_1} + \boldsymbol{U^\delta_2} \end{cases} \tag{19}$$

One has to keep in mind that the outer-pointing normal is defined as positive, thus explaining the last equation in the system of Eq. (19). The exponent δ is introduced to signify that the vectors

of the condensed pressure and normal velocity result from the prescribed velocity jump defined by Eq. (18). From Eq. (19), we can deduce:

$$\boldsymbol{P}^{\boldsymbol{\delta}}_{\mathbf{1+2}} = \boldsymbol{Z_1}\left(\boldsymbol{Z_1}+\boldsymbol{Z_2}\right)^{-1}\boldsymbol{Z_2}\boldsymbol{\delta U} \tag{20}$$

Since a velocity jump at the junction Ω corresponding to the condensation function φ^j is prescribed at the junction, this condensed pressure vector gives us the j^{th} column of the condensed impedance of the global system, $\boldsymbol{Z_{1+2}}$. We can then easily deduce the following relation:

$$\boldsymbol{Z_{1+2}} = \boldsymbol{Z_1}\left(\boldsymbol{Z_1}+\boldsymbol{Z_2}\right)^{-1}\boldsymbol{Z_2} \tag{21}$$

By inverting the previous equation, we finally obtain:

$$\boldsymbol{Z_1} = \boldsymbol{Z_2}\left(\boldsymbol{Z_2}-\boldsymbol{Z_{1+2}}\right)^{-1}\boldsymbol{Z_{1+2}} \tag{22}$$

3.4. Synthesis of the reverse CTF principle

In the previous sections, all the quantities needed for the application of the reverse CTF method were obtained from information concerning subsystem 2 and the global system 1+2. Finally, putting all this information together will allow us to estimate the pressure at a given point of the uncoupled subsystem 1.

The expression of the vector of the point condensed impedance, corresponding to the blocked pressure induced by a unitary monopole can be obtained by injecting the result of Eq. (22) into Eq. (16):

$$\boldsymbol{Z_1}(M_1) = \tilde{\boldsymbol{P}}^{\boldsymbol{M_1}}_{\mathbf{1}} = \left(\boldsymbol{I}+\boldsymbol{Z_2}\left(\boldsymbol{Z_2}-\boldsymbol{Z_{1+2}}\right)^{-1}\boldsymbol{Z_{1+2}}\boldsymbol{Z_2}^{-1}\right)\boldsymbol{P}^{\boldsymbol{M_1}}_{\mathbf{1+2}} \tag{23}$$

Ultimately, the pressure at point M_1 of the uncoupled subsystem 1 given by Eq. (12) can be rewritten as:

$$\tilde{p}_1(M_1) = p_{1+2}(M_1) + \left(\boldsymbol{I}+\boldsymbol{Z_2}\left(\boldsymbol{Z_2}-\boldsymbol{Z_{1+2}}\right)^{-1}\boldsymbol{Z_{1+2}}\boldsymbol{Z_2}^{-1}\right)\boldsymbol{P}^{\boldsymbol{M_1}}_{\mathbf{1+2}}\boldsymbol{Z_2}^{-1}\boldsymbol{P_{1+2}} \tag{24}$$

This final expression constitutes the main theoretical result of the present paper. It permits estimating the response at any point of subsystem 1 from the knowledge of quantities related to subsystem 2 and to the global system 1+2.

4. Numerical validation of the proposed reverse CTF approach

4.1. Test case definition

To validate and evaluate the accuracy of the reverse CTF method proposed in the previous section and based on Eqs. (22) and (24), we are going to compare the results obtained with the reverse CTF method to the reference results for an academic test case. The latter consists in the scattering problem of a rigid sphere in an infinite water domain, impacted by an acoustic plane wave. The choice of this test case was motivated by the fact that it constitutes a common and a reference case in the literature to study the acoustic scattering by an immersed object and that the principle of the proposed apporach is general and can be applied to various cases. Furthermore, the reference calculation, developped in [36] and based on the expansion of a plane wave in spherical harmonics, is an analytical solution easy to implement and gives accurate results with reasonable calculation costs. Moreover, for the "direct CTF" apporach, the coupling between the model of a water sphere and the model of a rigid sphere immersed in water can be qualified of strong coupling. Indeed, the behaviour of these subsystems when they are coupled together (corresponding to the model of an infinite water medium) is significantly different from those when they are uncoupled. Considering this case allows us to evaluate the ability of the "reverse CTF" apporach to decouple subsystems that are strongly coupled. As illustrated in figure 4, the reverse CTF approach will deal with this problem by removing a water sphere (i.e. the subsystem 2) from an infinite water domain (i.e. the global system 1+2). An infinite water domain with a rigid sphere will then be obtained (i.e. subsystem 1). In other words, from the condensed transfer functions of the infinite water domain and of the water sphere, we will deduce the acoustic scattering of the rigid sphere using subtractive modeling. The characteristics of the infinite domain and the sphere are given in table 1. The origin of the coordinates is taken at the center of the sphere, and the calculations will be conducted in the spherical coordinate system shown in figure 4.

For the purposes of comparison, a theoretical reference calculation is performed by developing the incident plane wave and the scattered pressure field in spherical harmonics, and by writing that the normal velocity at the surface of the sphere is null [36]. Harmonic responses are calculated from frequencies between 100 Hz and 1000 Hz, with a step of 1 Hz. This frequency range was considered to obtain the first two resonant frequencies of the water sphere (i.e. 497 Hz and 798 Hz) and its first anti-resonant frequency (i.e. 750 Hz). The limitation of the reference results is related to the

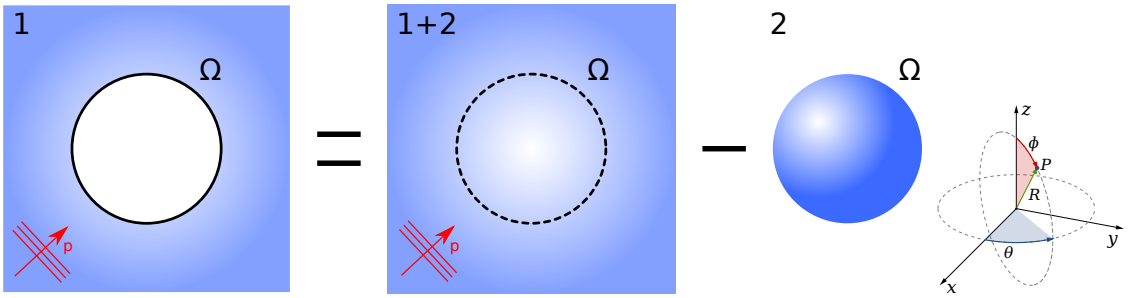

Figure 4: Illustration of the reverse CTF method principle applied to the scattering of a rigid sphere.

Parameter	**Notation**	**Value**	**Unit**
Radius	a	1	m
Density	ρ	1000	kg.m^{-3}
Sound speed	c_0	1500	m.s^{-1}
Loss factor	η	0	-

Table 1: Material characteristics and dimensions.

number of spherical harmonics considered in the calculation. After a trial and error test, it has been concluded that the calculations have converged in the frequency band of interest when $N = 40$ harmonics.

It is reminded here that the objective of this study is to validate from a practical point of view the subtractive modeling approach developped in section 3, and to study the influence of several parameters, as the type and the number of condensation functions. At this stage of the development of the proposed approach, it is then more relevant to focus on the validity and convergence of the approach rather than its computational performances compared to alternative ones. This is why the reference calculation of this application test is an analytical one and that there is no emphasis on the computational time of the proposed approach in this paper.

To apply the reverse CTF approach, in accordance with the theoretical backgrounds of section 3, the condensed impedances defined by Eq. (2) for subsystem 2 and Eq. (17) for the global system should be calculated. These quantities are related to the set of condensation functions, $\{\varphi^i\}_{1\leqslant i\leqslant N}$. Two types of condensation function are considered and presented in the next section before analyzing the results of the reverse CTF approach.

4.2. Two types of condensation functions

4.2.1. Weighted spherical harmonics

As developed in Appendix A, the pressure field in the infinite domain and in the sphere can be described as an infinite sum of so called spherical harmonics. Hence, for the condensed impedances, using spherical harmonics as condensation functions will result in a greatly simplified expression. The spherical harmonics are defined in spherical coordinates as:

$$\psi_{n,m}(\theta,\phi) = \sqrt{\frac{2n+1}{4\pi}\frac{(n-m)!}{(n+m)!}} P_n^m(\cos\theta)\mathrm{e}^{\mathrm{i}m\phi}, \quad n \in [\![0, N_L]\!], \quad m \in [\![-n, n]\!] \tag{25}$$

where P_n^m is the associated Legendre polynomial and N_L is the maximal degree of the associated Legendre polynomial. The condensation function φ^i associated with the spherical harmonic $\psi_{n,m}$ and called the weighted spherical harmonic is then defined at the surface of the sphere of radius a by:

$$\varphi^i = \frac{1}{a}\psi_{n,m}, \quad i \in [\![1, N]\!], \quad n \in [\![0, N_L]\!], \quad m \in [\![-n, n]\!] \tag{26}$$

The number of condensation functions N is directly linked to the maximal degree of the associated Legendre polynomial N_L by the following relation:

$$N = (N_L + 1)^2 \tag{27}$$

As an illustration, examples of spherical harmonics on the surface of the sphere are presented in figure 5. The condensation functions associated with the spherical harmonics form an orthonormal set for the scalar product in spherical coordinates at the surface of the sphere:

$$\left\langle \varphi^i, \varphi^j \right\rangle = \int_0^{2\pi}\int_{-\pi/2}^{\pi/2} \varphi^i \varphi^{j*} a^2 \sin\theta \,\mathrm{d}\theta \,\mathrm{d}\phi = \delta_{ij}, \tag{28}$$

with δ_{ij} being the Kronecker symbol, and * denoting the complex conjugate.

Applying the reverse CTF approach using spherical harmonics as condensation functions will result in considering condensed impedance matrices that are diagonal, as a result of the orthonormal properties of the spherical harmonics. This means that the contributions of the different condensation functions (i.e. the spherical harmonics) will be independent from one another. This constitutes a particular case but it can be useful for analyzing the results.

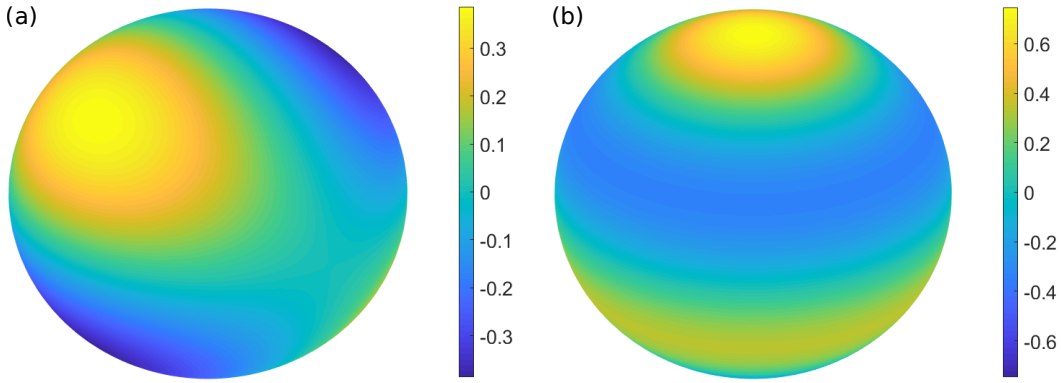

Figure 5: Examples of spherical harmonic functions. (a) $\psi_{2,1}$ (b) $\psi_{3,0}$

4.2.2. 2D gate functions

The second condensation functions investigated are the 2D gate functions $\varphi^i, i \in [\![1, N]\!]$. They are defined depending on their surface Ω_s as follows:

$$\varphi^i(\theta_s, \phi_s) = \begin{cases} \frac{1}{\sqrt{\Omega_s}} & \text{if} \quad \begin{cases} \theta_{i-1} \leqslant \theta_s < \theta_i \\ \phi_{i-1} \leqslant \phi_s < \phi_i \end{cases} \\ 0 \quad \text{elsewhere} \end{cases} \tag{29}$$

It can be easily verified that the condensation functions defined by Eq. (29) are orthonormal with the scalar product defined in Eq. (28). The four angles $\theta_{i-1}, \theta_i, \phi_{i-1}, \phi_i$ that appear in this expression are defined in figure 6a. They parametrize the corners of the patch i that can be linked to the i^{th} 2D gate function. The coupling surface Ω is then divided into N patches defining the N gate functions as condensation functions (CFs)(see figure 6b). The impedance between CF i and CF j corresponds to the mean pressure on the patch i when a unit prescribed normal velocity is imposed on patch j. Contrary to the spherical harmonics as CFs, the gate functions as CFs lead to non-diagonal condensed impedance matrices. In terms of matrix resolution, the latter case is more general than the former one. We also emphasize that the CTF approach considering this type of condensation function corresponds to the PTF approach described in the literature. Applying the reverse CTF approach in this case can therefore be considered as applying the reverse PTF approach.

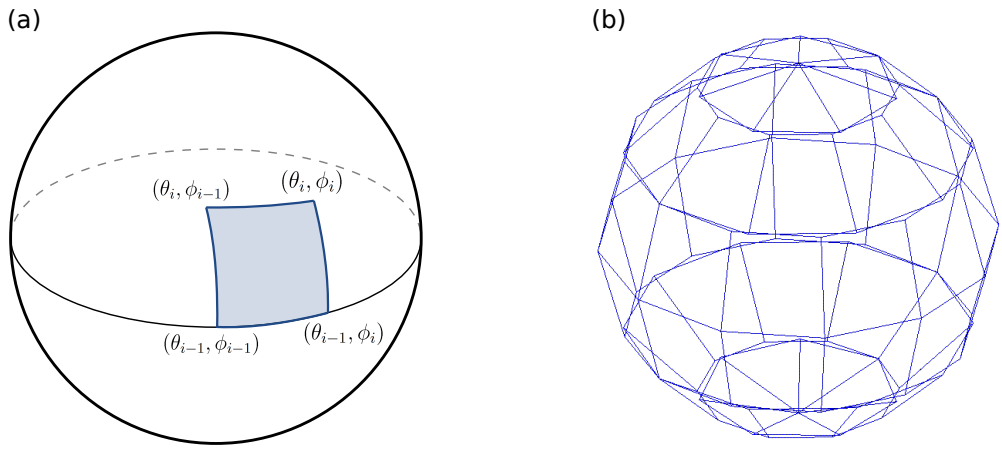

Figure 6: (a) Definition of a patch related to a 2D gate functions. (b) Definition of the patches over the sphere surface.

4.2.3. Calculation of the condensed transfer functions and convergence criteria

To apply the reverse CTF approach, the condensed impedances of the water sphere $\boldsymbol{Z_2}$ and the infinite water medium $\boldsymbol{Z_{1+2}}$ must be calculated. Moreover, to assess the accuracy of the method for evaluating the condensed impedances of the water sphere $\boldsymbol{Z_1}$ using Eq. (22), it is necessary to calculate $\boldsymbol{Z_1}$ directly to obtain a comparison point. The analytical calculations of these condensed impedances for both subsystems and for the global system are developed in Appendix A for the two types of condensation function. These calculations are based on a spherical harmonics decomposition of the pressure field in the water medium.

The number of condensation functions considered and thus of condensed impedances, plays a key role in the convergence of the CTF method [19, 21, 22]. According to the previous studies on the CTF method, a criterion equivalent to the Nyquist-Shannon sampling theorem assuming at least two points per wavelength to sample a signal should be applied. As the problem considered is purely acoustical, acoustic wavelength at the highest frequency of interest (i.e. 1000 Hz), $\lambda_{\min} = 1.5$ m should be considered for the criterion. For the weighted spherical harmonics as CFs, the maximal degree of the Legendre polynomial N_L related to Eq. (26) should respect the criterion [19]:

$$N_L \geqslant \frac{2\pi a}{\lambda_{\min}} \tag{30}$$

In the present case, this criterion yields $N_L = 5$, giving us a number of CFs equal to $N = 36$

(following Eq. (27)). For the 2D gate functions as CFs, the size d of the patches should be smaller than half the smallest wavelength:

$$d < \frac{\lambda_{\min}}{2} \tag{31}$$

In order to be compliant with this criterion, the sphere is divided into 58 patches, with 12 patches on the principal circumference. The patches considered in the following calculations are those displayed in figure 6b). It can be seen that the patches on the top and the bottom of the sphere take the shape of triangles instead of trapezoids for the other patches, and that the nodes between two consecutive patches are not necessarily coincident. However, these geometrical particularities concerning the patches do not have any influence on the results of the PTF method [18]. It can be noticed that the number of CFs considered with the weighted spherical harmonics is lower than that considered with the 2D gate functions. This is due to the fact that the size of some patches is well below the criterion [18], because of geometrical constraints.

According to the calculation of the condensed impedances for the 2D gate functions as CFs in Appendix A, their expressions (see Eq. (A.14), Eq. (A.18) and Eq. (A.22)) depend on an infinite sum of spherical harmonics. In practice, these series must be truncated to a finite value N_L^{2D}, corresponding to the maximal degree of the associated Legendre polynomials of the spherical harmonics decomposition of the pressure fields. The value of N_L^{2D} influences the convergence and the cost of the calculation of the condensed impedances. After trial and error tests, it was found that using N_L^{2D}=50 is a good compromise in order to converge correctly without being too numerically heavy. We underline here that this parameter is related to the method of evaluating the condensed impedances and does not directly concern the convergence of the CTF or reverse CTF approaches characterized by the criteria [19].

4.3. Decoupling for the condensed impedances

4.3.1. Results

As a first validation, the condensed impedances of subsystem 1, $\boldsymbol{Z_1}$, obtained from $\boldsymbol{Z_2}$, $\boldsymbol{Z_{1+2}}$ and the decoupling formula of Eq. (22), are compared to the results of the analytical expression of $\boldsymbol{Z_1}$ given in Eq. (A.21) for the weighted spherical harmonics, and Eq. (A.22) for the 2D gate functions.

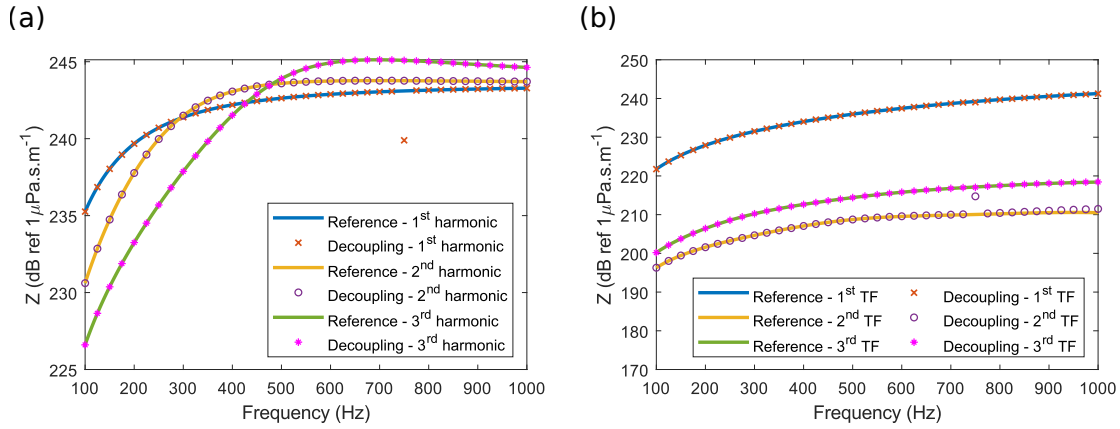

Figure 7: Comparison between the condensed impedances computed analytically (i.e. reference) and with the reversed CTF approach. (a) Weighted spherical harmonics. (b) 2D gate functions.

The comparison is proposed in figure 7. The comparison for 3 weighted spherical harmonics as CFs (respectively the couples $(n,m) = (0,0), (n,m) = (1,0), (n,m) = (2,0)$) are plotted in figure 7a). A perfect match can be seen between the reverse CTF approach and the reference calculation, except for a single frequency at 750 Hz for the first spherical harmonic. The reasons for this discrepancy at this particular frequency will be studied in the next section.

Concerning the comparison for 2D gate functions as CFs, figure 7b) shows the results for 3 different condensed transfer functions (TFs) in order to sweep different possibilities:

- the first TF is a direct impedance on a trapezoid patch : the excitation patch and the observation patch are the same.
- the second TF is a crossed impedance between two trapezoid patches that are widely separated one from another.
- the third TF is a crossed impedance between a trapezoid patch and a triangular patch that are close to each other.

As with the weighted spherical harmonics, the comparison between the reference curves and the reverse CTF curves show a quasi-perfect match, except for the second transfer function for which an error appears at 750 Hz (as in figure 7a for the weighted spherical harmonics as CFs).

In the following subsection, the numerical sensitivity of the method will be investigated to identify the possible sources of this error at 750 Hz.

4.3.2. Analysis of numerical sensitivity

The application of Eq. (22) related to the reverse CTF method involves the inversion of the subtraction of the impedance matrices, $\boldsymbol{Z_2} - \boldsymbol{Z_{1+2}}$. This inversion can imply numerical instabilities. The sensitivity of the matrix inversion to the numerical errors can be characterized by the condition number. Particularly high values indicate that the problem is ill-conditioned and sensitive to numerical errors.

In figure 8, the condition numbers of the impedance matrix of subsystem 2 and subsystem 1+2, as well as their differences, are plotted as a function of frequency for the weighted spherical harmonics. As the condensed impedance matrices are diagonal in this case, the condition number corresponds to the ratio between the largest value on the diagonal and the smallest one. It appears that for each of the matrices investigated, the problem is particularly ill-conditioned at 750 Hz, which was the critical frequency identified in the previous subsection. It can also be noted that for $\boldsymbol{Z_2}$ and $\boldsymbol{Z_2} - \boldsymbol{Z_{1+2}}$, two other frequencies show high condition numbers, around 500 Hz and 800 Hz. These two particular frequencies correspond to the resonant frequencies of the water sphere. As these frequencies are clearly identified and no significant error can be observed at these frequencies in the figure, they will not be investigated.

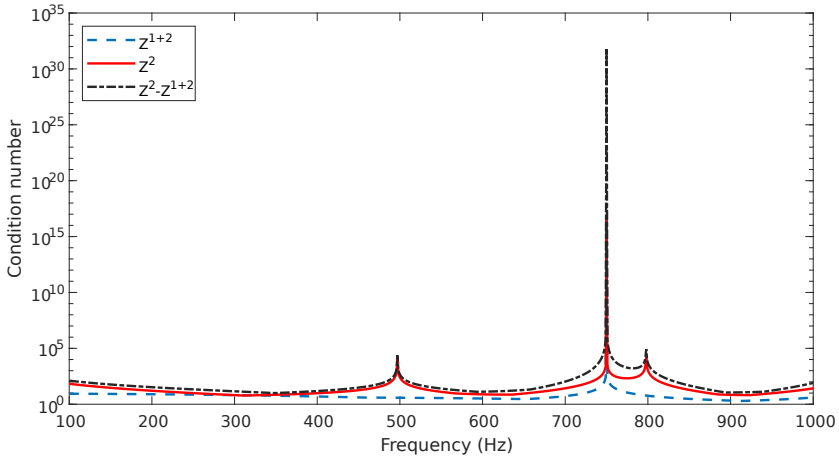

Figure 8: Condition number of the condensed impedances: case of the weighted spherical harmonics as CFs.

As the problem encountered in figure 7a) appears only on the condensed impedance associated with the first spherical harmonic, the first condensed impedances of subsystems 2 and 1+2 are

shown in figure 9. It can be seen that for both systems, an anti-resonant phenomenon appears at 750 Hz (i.e. the impedances tend toward zero). Looking at Eq. (A.17) and Eq. (A.13) reveals that this anti-resonant phenomenon is due to the first spherical Bessel function of the first kind that cancels at this frequency. In addition, since the two condensed impedances have the same value at this frequency, the subtraction of the two matrices that appear in Eq. (22) is also null. This explains the particularly high value of the condition number and the numerical errors observed previously. The same analysis was carried out with the 2D gate functions as CFs. The condition number also presents significant values for the two resonance frequencies of the water sphere and a very high value at 750 Hz, identified as a non-resonant frequency of the water sphere. Since the analysis leads to the same conclusions as for the weighted spherical harmonics, the results are not plotted here.

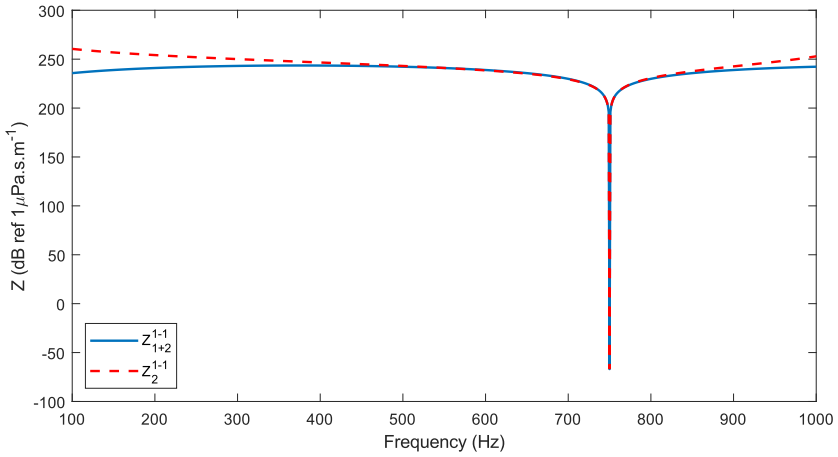

Figure 9: Comparison of the 1st condensed impedance of subsystems 2 and 1+2 (weighted spherical harmonics as CFs).

As stated in table 1, the previous calculations were performed considering a null damping loss factor for the fluid domain that constitutes the theoretical case. We observed that the absence of damping in the model leads to the high numerical instabilities encountered, especially around the anti-resonant frequency. In practice, acoustic waves are slightly attenuated during their propagation due to dissipative effects (viscosity and thermal conductivity). In order to consider this physical phenomenon and to evaluate the impact of the damping on the numerical sensitivity of the method,

slight damping is introduced in the model through a complex acoustic wavenumber:

$$k_0^* = k_0(1 - \mathrm{i}\eta) \tag{32}$$

where i is the complex number $\mathrm{i}^2 = -1$.

In the following part of the study, the damping loss factor of the water is set to $\eta = 0.001$. The condition numbers related to the impedance matrices were recalculated by considering this slight damping and are shown in figure 10. It is noteworthy that the values were greatly reduced in general and for the critical frequencies in particular, compared to the case without damping. The inverted matrix $\boldsymbol{Z_2} - \boldsymbol{Z_{1+2}}$ is still ill-conditioned at the anti-resonant frequency, but to a much smaller extent.

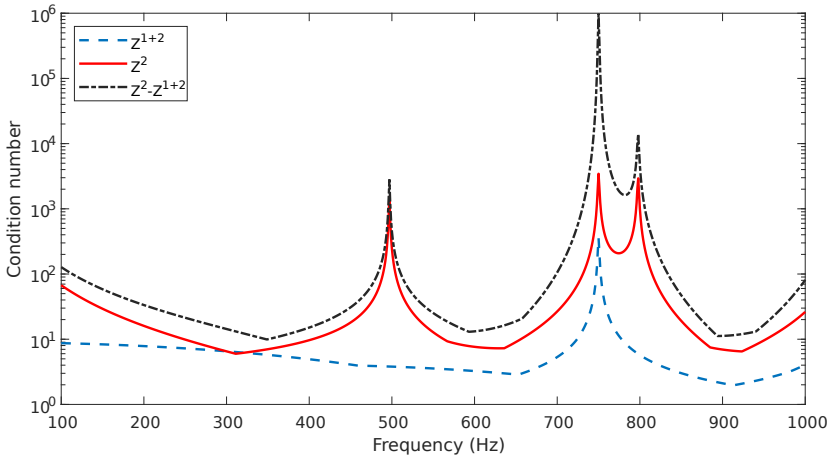

Figure 10: Condition number of the condensed impedances with a slight damping (weighted spherical harmonics as CFs).

As the condition number was significantly reduced by adding damping in the model, we can expect to obtain accurate results with the reversed CTF approach over the whole frequency range of interest. This is verified in figure 11. The errors observed in figure 7 for the case without damping are not observed for the case with slight damping. This result is valid for the two types of condensation function considered in this paper.

It can be concluded from this study that the decoupling formula in Eq. (22) is validated numerically for the practical case including a slight damping in the water medium (i.e. for the

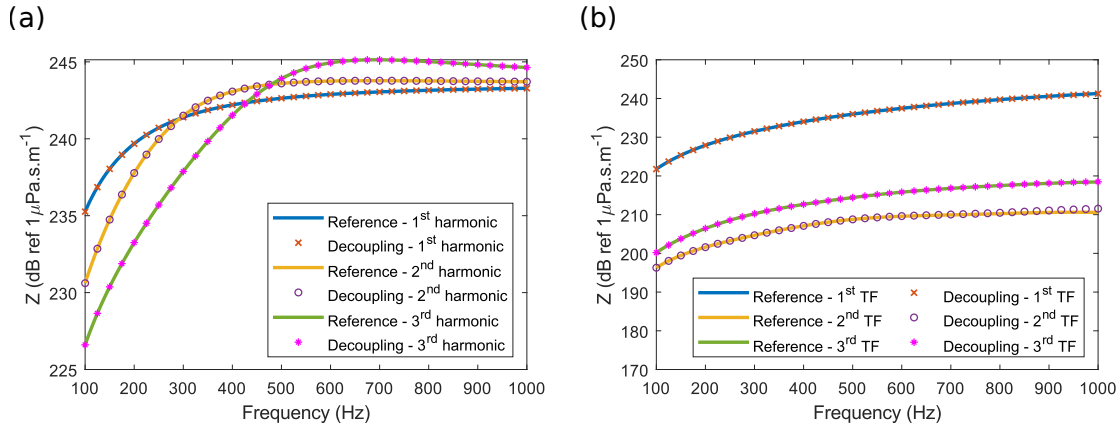

Figure 11: Comparison between the condensed impedances computed analytically (i.e. reference) and with the reversed CTF approach. Case with a slight damping in the model. (a) Weighted spherical harmonics. (b) 2D gate functions.

non-conservative system). The dissipative effect allows to avoid the numerical errors at the anti-resonant frequency of the water sphere that were observed for the case without damping (i.e. the conservative system).

4.4. Decoupling for the pressure at a given point into the fluid domain

Now, let us focus on assessing the reverse CTF approach to predict the pressure at a given point using the formula in Eq. (24). To do that, we consider the scattering problem of a plane wave impacting a rigid sphere. This case was intensively studied in litterature [36]. In the following section, the principle of this calculation used as reference will be recalled before comparing its results with the reverse CTF approach.

4.4.1. Theoretical calculation

In spherical coordinates, the pressure field of a plane wave of angular frequency ω travelling in the direction ($\theta = \pi$, $\phi = 0$) can be defined by:

$$p_i(R, \theta) = P_i \mathrm{e}^{\mathrm{i}k_0 R \cos\theta} \tag{33}$$

with P_i being the amplitude of the plane wave, and k_0 the acoustic wavenumber in the fluid domain. The expression in Eq. (33) can be expanded in spherical harmonics using Legendre polynomials:

$$p_i(R,\theta) = P_i \sum_{n=0} (2n+1)\,\mathrm{i}^n P_n(\cos\theta)\, j_n(k_0 R) \tag{34}$$

with $P_n(\cos\theta)$ the Legendre polynomial, and j_n the spherical Bessel function of the first kind.

Considering the solutions in the spherical coordinates of the homogeneous Helmholtz equation and the homogeneous Euler equation at the surface of the sphere, we can calculate the pressure scattered by the rigid sphere of radius a [36]:

$$p_{s\infty}(R,\theta) = -P_i \sum_{n=0} (2n+1)\,\mathrm{i}^n P_n(\cos\theta)\, \frac{j_n'(k_0 a)}{h_n'(k_0 a)} h_n(k_0 R) \tag{35}$$

where h_n is the spherical Hankel function of the first kind, and j_n' and h_n' are the derivatives of the spherical Bessel function of the first kind and the spherical Hankel function of the first kind with respect to their argument, respectively. The total pressure field in the medium is thus the addition of the incident and the scattered pressures $p_{\text{tot}} = p_i + p_{s\infty}$ which gives:

$$p_{\text{tot}}(R,\theta) = P_i \sum_{n=0}^{40} (2n+1)\,\mathrm{i}^n P_n(\cos\theta) \left[j_n(k_0 R) - \frac{j_n'(k_0 a) h_n(k_0 R)}{h_n'(k_0 a)} \right] \tag{36}$$

4.4.2. Comparison

To apply the decoupling formula in Eq. (24) to predict the pressure at any point M_1 in the fluid domain, we must still evaluate $\boldsymbol{P_{1+2}}$, the condensed pressure vector induced by the acoustic plane wave and $\boldsymbol{P_{1+2}^{M_1}}$, the condensed pressure vector induced by a monopole source located at point M_1 and of unit volume velocity. The details of the calculations are given in Appendix B. First, the decoupling formula in Eq. (24) is tested using the weighted spherical harmonics as condensation functions, by evaluating the pressure at a given point of the domain over the frequency range of interest. This calculation is also a means of evaluating the criterion proposed in Eq. (30), related to the maximal degree of the associated Legendre polynomial N_L. The results are presented in figure 12 for 4 different points, to account for different possibilities regarding the angle and the distance to the surface of the sphere. The quantity plotted here is the sound pressure level (SPL), in dB, the reference sound pressure being $p_0 = 1$ μPa:

$$L_p = 20 \log\left(\frac{p}{p_0}\right) \tag{37}$$

For each point, the reverse CTF method is applied with 3 different values of N_L to evaluate the convergence of the method regarding the criterion defined. In section 4.2.3, the criterion in Eq. (30) yielded $N_L = 5$, corresponding to $N = 36$ condensation functions. The results are also presented for $N_L = 3$ and $N_L = 7$, corresponding to $N = 16$ and $N = 64$ condensation functions, respectively. Both calculations were carried out considering a damping loss factor, $\eta = 0.001$.

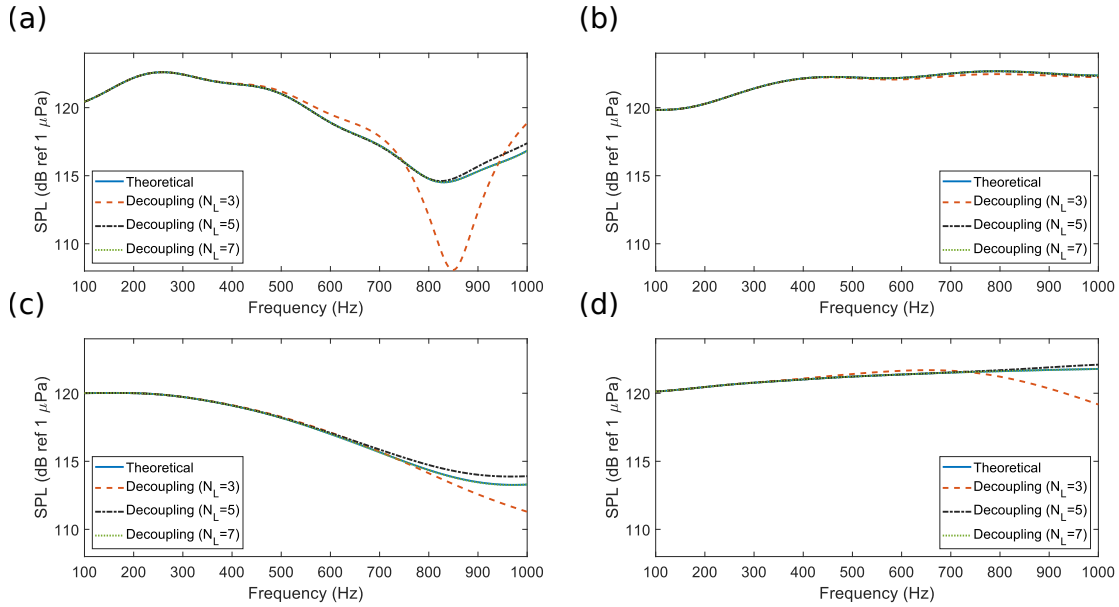

Figure 12: Pressure scattered by the rigid sphere - Comparison between the theoretical results and the reversed CTF results for 4 different points with the weighted spherical harmonics as CFs. (a) $r = 1.5$ m, $\theta = 180°$; (b) $r = 1.3$ m, $\theta = 103°$; (c) $r = 1$ m, $\theta = 30°$; (d) $r = 1.5$ m, $\theta = 0°$.

The results displayed in figure 12 show that the convergence criterion proposed in Eq. (30) is verified, because the evolution of the pressure for each evaluated point is described correctly, with errors that never exceed 1 dB. The results with $N_L = 3$ clearly show that taking fewer condensation functions than the criterion defined leads to large errors, while the results with $N_L = 7$ are very accurate, but required an increase in computation time. Finally, we can conclude that the results obtained with $N_L = 5$ are very satisfactory, both in terms of accuracy and computation time, and the criterion in Eq. (30) is validated from a practical point of view.

In the following, the calculation of the scattered pressure in the domain is carried out using the

2D gate functions as condensation functions, using the definition of the patches at the surface of the sphere presented in figure 6b. The results obtained with the method proposed (i.e. Eq. (24)) can be compared to the theoretical results given by Eq. (36). The map of the sound pressure level (in dB ref 1 μPa according to equation 37) around the sphere is presented in figure 13 for the 2 calculations and for 3 different frequencies:

- f_1=497 Hz corresponds to the first resonant frequency of the water sphere.
- f_2=750 Hz corresponds to an anti-resonant frequency.
- f_3=1000 Hz corresponds to the highest calculated frequency.

The latter allows us to verify if the method converges correctly when the criterion is applied whereas the first two correspond to the critical frequencies already evoked in the previous section.

For all the graphs, the plane wave is travelling towards the positive x direction and reaches the sphere at $x = -1$. The graphs on the left hand side show the results of the theoretical calculation (i.e. Eq. (36)), while the figures on the right hand side show the results of the decoupling calculation (i.e. Eq. (24)). As for the weighted spherical harmonics, both calculations were carried out considering a damping loss factor $\eta = 0.001$.

All the graphs display a similar global behavior, with a maximum pressure around the point of impact of the plane wave with the sphere (i.e. $(x, y) = (-1, 0)$ while the minimum pressures are located in the shadow zone of the sphere (around $\theta = \pi/6$) and in a zone before the point of impact (between $x = -1.2$ and $x = -2$) where destructive interferences seem to appear.

The comparison shows a very good agreement between the two calculations. Minor errors occur in the shadow zone of the sphere, and several numerical discontinuities occur at the maximum frequency, but the errors never exceed 1 dB. One has to be aware that the different fields of interest in this study (acoustic pressure, acoustic velocity) exhibit continuous properties. However, as described in Eq. (1), these fields are approximated on the basis of the condensation functions which, in the present case, are discontinuous (following the definition of the patches in Eq. (29)). Hence, the decomposition of continuous fields on the basis of discontinuous functions leads to slightly rougher approximations than the decomposition on the weighted spherical harmonics displayed on figure 12, thus explaining the numerical discontinuities occuring at the maximum frequency. These discontinuities are thus not related to the number of condensation functions nor the convergence

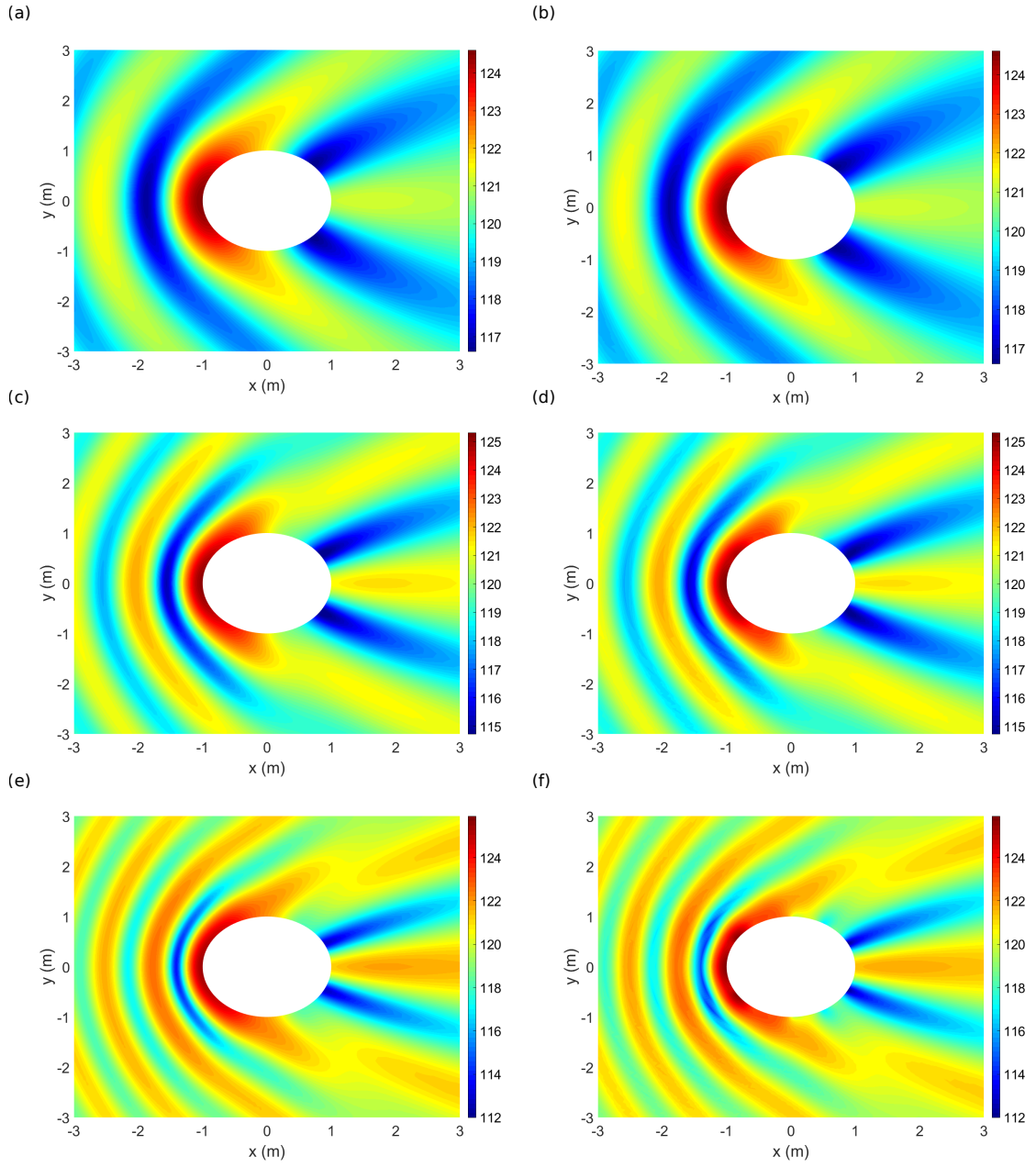

Figure 13: Pressure scattered by the rigid sphere (SPL in dB ref 1 μPa) - Comparison between the theoretical results (a,c,e) and the reversed CTF results using 2D gate functions as CFs (b,d,f) for 3 frequencies: (a,b), 497 Hz; (c,d), 750 Hz; (e,f), 1000 Hz.

criterion proposed in Eq. (31). Finally, we can affirm that these results are very satisfactory and thus we can conclude on the validity of the proposed developments.

5. Conclusion

In the present paper, the principle of a subtractive modeling technique that can be used to decouple a subsystem from a global system was established. This approach can be used to modify or perturbate an existing model (for instance an analytical model), and is based on a reverse formulation of the Condensed Transfer Function method usually used to predict the behavior of coupled subsystems from transfer functions defined for each subsystem. Eqs. (22) and (24) constitute the fundaments of the proposed approach. The approach is versatile and can be applied not only to acoustic problems, but also to vibrational or vibroacoustic problems as the direct CTF approach has already shown its ability in dealing with such problems [20, 21, 43].

The formulation was validated numerically in the case of a rigid sphere immersed in water and impacted by a plane wave. Using acoustic models of the infinite water medium and of the water filled sphere, the proposed approach allowed predicting the behavior of the rigid sphere immersed in water. Comparisons of the results with theoretical calculations led to the numerical validation of the approach for two types of condensation functions, namely weighted spherical harmonics and 2D gate functions. For the case without damping, it was observed that numerical instabilities occur for frequencies around the anti-resonance of the water sphere. However, these instabilities disappear as soon as slight damping is introduced in the model, as it occurs in real situation due to viscosity and thermal conductivity.

Acknowledgments

This work was funded by Naval Group Research and performed within the framework of the LabEx CeLyA (ANR-10-LABX-0060) of Université de Lyon, within the program "Investissements d'Avenir" (ANR-16-IDEX-0005) operated by the French National Research Agency.

Appendix A. Calculation of the condensed transfer functions

Appendix A.1. Condensed impedances of the global system 1+2

In order to calculate the condensed impedances of the infinite water domain 1+2 (see figure 4), and in accordance with its definition in Eq. (17), a normal velocity jump φ^i is imposed on the spherical surface Ω. The resulting pressure on the surface is estimated using a spherical harmonics decomposition [44], considering two domains: D^+, the volume outside the surface of the sphere of radius a, and D^-, the volume inside the surface of the sphere. It is written:

$$p^+(R,\theta,\phi) = \sum_{n=0}^{+\infty} \sum_{m=-n}^{n} \psi_{n,m}(\theta,\phi) \left[A^+_{n,m} h^{(1)}_n(k_0 R) + B^+_{n,m} h^{(2)}_n(k_0 R) \right], \text{ for } R \geqslant a \tag{A.1a}$$

$$p^-(R,\theta,\phi) = \sum_{n=0}^{+\infty} \sum_{m=-n}^{n} \psi_{n,m}(\theta,\phi) \left[A^-_{n,m} j_n(k_0 R) + B^-_{n,m} y_n(k_0 R) \right], \text{ for } 0 \geqslant a \geqslant R \tag{A.1b}$$

where $h^{(1)}_n$ and $h^{(2)}_n$ are the spherical Hankel functions of the first and second kind, respectively, and j_n and y_n are the spherical Bessel functions of the first and second kind, respectively. k_0 is the acoustic wavenumber and $\psi_{n,m}(\theta,\phi)$ are the spherical harmonics defined in Eq. (25).

Applying the boundary conditions at infinity (divergent waves) and at the center of the sphere (convergent waves) to the properties of the spherical Hankel and Bessel functions yields:

$$\begin{cases} B^+_{n,m} = 0 \\ B^-_{n,m} = 0 \end{cases} \tag{A.2}$$

The pressure fields in the domains D^+ and D^- are thus:

$$p^+(R,\theta,\phi) = \sum_{n=0}^{+\infty} \sum_{m=-n}^{n} \psi_{n,m}(\theta,\phi) A^+_{n,m} h^{(1)}_n(k_0 R), \text{ for } R \geqslant a \tag{A.3a}$$

$$p^-(R,\theta,\phi) = \sum_{n=0}^{+\infty} \sum_{m=-n}^{n} \psi_{n,m}(\theta,\phi) A^-_{n,m} j_n(k_0 R), \text{ for } 0 \geqslant a \geqslant R \tag{A.3b}$$

A velocity jump δu is imposed on the surface of the sphere, such that the impedance is given by $Z = p/\delta u$. The pressure continuity and velocity equilibrium conditions at the surface of the sphere (i.e. $R = a$) are then written:

$$\begin{cases} p^+(a,\theta,\phi) = p^-(a,\theta,\phi) \\ \delta u = u^+(a,\theta,\phi) + u^-(a,\theta,\phi) \end{cases} \tag{A.4}$$

The second equation of A.4 takes into account the orientation of the normals, as in the section 3.3, with the normal pointing in the outer-direction of the considered domain. The pressure and the radial velocity are linked by the Euler relation:

$$u_n = -\frac{1}{\mathrm{i}\omega\rho}\frac{\partial p}{\partial r} \tag{A.5}$$

With the orientation of the normals previously defined, we can write:

$$\begin{cases} u^+(a,\theta,\phi) = -u_n \\ u^-(a,\theta,\phi) = u_n \end{cases} \tag{A.6}$$

Furthermore, the spherical Hankel and Bessel functions can be derived with respect to their argument according to the following relation:

$$\frac{\partial f_n}{\partial x}(x) = \frac{n}{x} f_n(x) - f_{n+1}(x) \tag{A.7}$$

In the following, and in order to clarify the equations, the spherical Hankel function of the first kind $h_n^{(1)}$ is noted h_n. Combining Eq. (A.3a) and Eq. (A.3b) with the relations in Eq. (A.4) and Eq. (A.5) yields:

$$\sum_{n=0}^{+\infty}\sum_{m=-n}^{n} \psi_{n,m}(\theta,\phi)\, A^+_{n,m} h_n(k_0 a) = \sum_{n=0}^{+\infty}\sum_{m=-n}^{n} \psi_{n,m}(\theta,\phi)\, A^-_{n,m} j_n(k_0 a) \tag{A.8a}$$

$$\delta u = \frac{k_0}{\mathrm{i}\omega\rho}\sum_{n=0}^{+\infty}\sum_{m=-n}^{n} \psi_{n,m}(\theta,\phi)\left[A^+_{n,m} h'_n(k_0 a) - A^-_{n,m} j'_n(k_0 a)\right] \tag{A.8b}$$

Using the orthonormal properties of the spherical harmonics (see Eq. (28)), we can multiply Eq. (A.8a) and Eq. (A.8b) by $\psi_{\nu,\mu}$ and integrate them on the surface of the sphere to eliminate the sums:

$$\begin{cases} A^+_{n,m} h_n(k_0 a) = A^-_{n,m} j_n(k_0 a) \\ \iint_\Omega \delta u \cdot \psi^*_{\nu,\mu}(\theta,\phi) a^2 \sin\theta d\theta d\phi = \frac{k_0 a^2}{\mathrm{i}\omega\rho}\left[A^+_{n,m} h'_n(k_0 a) - A^-_{n,m} j'_n(k_0 a)\right] \end{cases} \tag{A.9}$$

where * denotes the complex conjugate. In order to calculate the condensed impedances, the velocity jump must correspond to a condensation function φ^i, which are either weighted spherical harmonics or 2D gate functions, which means:

$$\iint_{\Omega} \delta u \cdot \psi^*_{n,m}(\theta,\phi) a^2 \sin\theta d\theta d\phi = \iint_{\Omega} \varphi^i \cdot \psi^*_{n,m}(\theta,\phi) a^2 \sin\theta d\theta d\phi = \varepsilon^i_{n,m}(a) \tag{A.10}$$

The evaluation of the factor $\varepsilon^i_{n,m}$, which depends on the the radius a of the sphere, will be evaluated for each type of CF. Eq. (A.9) now becomes:

$$\begin{cases} A^+_{n,m} h_n(k_0 a) = A^-_{n,m} j_n(k_0 a) \\ \varepsilon^i_{n,m}(a) = \frac{k_0 a^2}{\mathrm{i}\omega\rho} \left[A^+_{n,m} h'_n(k_0 a) - A^-_{n,m} j'_n(k_0 a) \right] \end{cases} \tag{A.11}$$

The resolution of this system of equations enables us to obtain the pressure at the surface of the sphere for the infinite domain:

$$p(a,\theta,\phi) = \omega\rho k_0 \sum_{n=0}^{+\infty} \sum_{m=-n}^{n} \psi_{n,m}(\theta,\phi)\, j_n(k_0 a) h_n(k_0 a) \varepsilon^i_{n,m}(a) \tag{A.12}$$

For each CF, the pressure must be projected on the CF φ^j to obtain the condensed impedance, according to Eq. (17). For the weighted spherical harmonics, it yields:

$$Z^{ij}_{1+2} = \begin{cases} \omega\rho k_0 a^2 j_i(k_0 a) h_i(k_0 a) & \text{if} \quad i = j \\ 0 & \text{elsewhere} \end{cases} \tag{A.13}$$

The form of this expression is explained by the orthonormal properties of the spherical harmonics, thus resulting in a diagonal condensed impedance matrix. As for the 2D gate functions, the condensed impedances of the global system 1+2 is given by:

$$Z^{ij}_{1+2} = \omega\rho k_0 \cdot \sum_{n=0}^{+\infty} \sum_{m=-n}^{n} j_n(k_0 a) h_n(k_0 a) \varepsilon^i_{n,m}(a) \varepsilon^{j*}_{n,m}(a) \tag{A.14}$$

Appendix A.2. Condensed impedances of the subsystem 2

In order to calculate the condensed impedances of the water sphere and in accordance with its definition in Eq. (2), a normal velocity is imposed on the spherical surface Ω (where the positive outer-pointing normal points towards the exterior of the sphere), corresponding to a condensation function: $u = \varphi^i$. The calculation process to estimate the resulting pressure is therefore similar to

that carried out in the previous section, except that the calculation is performed only inside the sphere. The pressure inside the sphere is given by Eq. (A.1b), whereas the Euler equation on the surface Ω yields (taking into account the orientation of the outer-pointing normal):

$$\varphi^i = -\frac{1}{\mathrm{i}\omega\rho}\frac{\partial p}{\partial r} \tag{A.15}$$

The pressure at the surface Ω of the sphere is easily derived:

$$p(a,\theta,\phi) = -\frac{\mathrm{i}\omega\rho}{k_0 a^2}\sum_{n=0}^{+\infty}\sum_{m=-n}^{n}\psi_{n,m}(\theta,\phi)\frac{j_n(k_0 a)}{j_n'(k_0 a)}\varepsilon^i_{n,m}(a) \tag{A.16}$$

As with the previous section, and following the definition of the condensed impedances of Eq. (2), the condensed impedances at the surface of the sphere for the weighted spherical harmonics are given by:

$$Z_2^{ij} = \begin{cases} -\frac{\mathrm{i}\omega\rho}{k_0}\frac{j_i(k_0 a)}{j_i'(k_0 a)} & \text{if} \quad i = j \\ 0 & \text{elsewhere} \end{cases} \tag{A.17}$$

As for the 2D gate functions, the condensed impedances are:

$$Z_2^{ij} = -\frac{\mathrm{i}\omega\rho}{k_0 a^2}\sum_{n=0}^{+\infty}\sum_{m=-n}^{n}\frac{j_n(k_0 a)}{j_n'(k_0 a)}\varepsilon^i_{n,m}(a)\varepsilon^{j*}_{n,m}(a) \tag{A.18}$$

Appendix A.3. Condensed impedances of the subsystem 1

The analytical condensed impedances of the infinite fluid domain bounded by the spherical surface Ω (subsystem 1 on figure 4) are calculated to validate and evaluate the ability of the reverse CTF method. As defined in Eq. (2), a normal velocity is imposed on the surface Ω (where the positive outer-pointing normal now points towards the center of the sphere), corresponding to a condensation function: $u = \varphi^i$. The pressure inside the water domain bounded by the surface Ω is described by Eq. (A.1a), whereas the Euler equation on the surface Ω yields (taking into account the orientation of the outer-pointing normal):

$$\varphi^i = \frac{1}{\mathrm{i}\omega\rho}\frac{\partial p}{\partial r} \tag{A.19}$$

Again, we derive the pressure at the surface Ω of the sphere:

$$p(a,\theta,\phi) = \frac{\mathrm{i}\omega\rho}{k_0 a^2}\sum_{n=0}^{+\infty}\sum_{m=-n}^{n}\psi_{n,m}(\theta,\phi)\,\frac{h_n(k_0 a)}{h_n'(k_0 a)}\varepsilon_{n,m}^{i}(a) \tag{A.20}$$

As with the previous sections, and following the definition of the condensed impedances of Eq. (2), the condensed impedances at the surface of the sphere for the weighted spherical harmonics are given by:

$$Z_1^{ij} = \begin{cases} \frac{\mathrm{i}\omega\rho}{k_0}\frac{h_i(k_0 a)}{h_i'(k_0 a)} & \text{if} \quad i=j \\ 0 & \text{elsewhere} \end{cases} \tag{A.21}$$

As for the 2D gate functions, the condensed impedances are:

$$Z_1^{ij} = \frac{\mathrm{i}\omega\rho}{k_0 a^2}\sum_{n=0}^{+\infty}\sum_{m=-n}^{n}\frac{h_n(k_0 a)}{h_n'(k_0 a)}\varepsilon_{n,m}^{i}(a)\varepsilon_{n,m}^{j*}(a) \tag{A.22}$$

Appendix B. Calculation of the condensed pressures

Appendix B.1. Condensed pressure induced by a unit monopole

In order to calculate $\boldsymbol{P}_{\mathbf{1+2}}^{\boldsymbol{M_1}}$, the condensed pressure vector induced by a monopole of unit volume velocity located at point M_1 into the infinite water domain 1+2, the expression of the free-space Green's function is expanded in spherical harmonics [36]. The acoustic field pressure at any point $\boldsymbol{M}(R,\theta,\phi)$ due to a spherical source located at point $\boldsymbol{M_1}(R_1,\theta_1,\phi_1)$ is given by:

$$p_i^{M_1} = \mathrm{i}\omega\rho\frac{\mathrm{e}^{\mathrm{i}k_0|\boldsymbol{M}-\boldsymbol{M_1}|}}{4\pi|\boldsymbol{M}-\boldsymbol{M_1}|} \tag{B.1}$$

where $|\bullet|$ represents the Euclidean norm.

Expanding this expression in spherical harmonics, the pressure induced by the monopole can be rewritten:

$$\begin{aligned} p_i^{M_1} = \frac{\omega\rho k_0}{4\pi}\sum_{n=0}^{+\infty}\sum_{m=0}^{n}\kappa_m\frac{(n-m)!}{(n+m)!}(2n+1)\cos\left(m(\phi-\phi_1)\right) \\ \cdot P_n^m(\cos\theta)\,P_n^m(\cos\theta_1)\,j_n(k_0 R)h_n(k_0 R_1) \end{aligned} \tag{B.2}$$

where

$$\kappa_m = \begin{cases} 1 & \text{if} \quad m = 0 \\ 2 & \text{if} \quad m \neq 0 \end{cases} \tag{B.3}$$

According to the definition of the condensed pressure, the pressure at the surface of the sphere (i.e. $R = a$) is projected on the condensation functions according to the scalar product in spherical coordinates defined in Eq. (28). For the weighted spherical harmonics as condensation functions, the i^{th} component of $\boldsymbol{P}_{\mathbf{1+2}}^{\boldsymbol{M_1}}$ is given by:

$$\begin{aligned} P_{1+2,i}^{M_1} = \langle p_i, \psi_{\nu,\mu} \rangle = \frac{\omega \rho k_0}{(4\pi)^{3/2}} \sum_{n=0}^{+\infty} \sum_{m=0}^{n} \kappa_m \frac{(n-m)!}{(n+m)!} (2n+1) \sqrt{(2\nu+1) \cdot \frac{(\nu-\mu)!}{(\nu+\mu)!}} \\ \cdot P_n^m(\cos\theta_1)\, j_n(k_0 a) h_n(k_0 R_1) \\ \cdot \iint_{\Omega} \cos(m(\phi-\phi_1))\, \mathrm{e}^{-\mathrm{i}\mu\phi} P_n^m(\cos\theta)\, P_\nu^\mu(\cos\theta)\, a \sin\theta \,\mathrm{d}\theta \,\mathrm{d}\phi \end{aligned} \tag{B.4}$$

where $\psi_{\nu,\mu}$ corresponds to the i^{th} condensation function, as defined in Eq. (26).

For the 2D gate functions as condensation function, the i^{th} component of $\boldsymbol{P}_{\mathbf{1+2}}^{\boldsymbol{M_1}}$ is given by:

$$\begin{aligned} P_{1+2,i}^{M_1} = \left\langle p_{inc}^{M_1}, \varphi^i \right\rangle = \frac{\omega \rho k_0}{4\pi} \sum_{n=0}^{+\infty} \sum_{m=0}^{n} \kappa_m \frac{(n-m)!}{(n+m)!} (2n+1) P_n^m(\cos\theta_1)\, j_n(k_0 a) h_n(k_0 R_1) \\ \cdot \frac{1}{\sqrt{\Omega_i}} \iint_{\Omega_i} \cos(m(\phi-\phi_1))\, P_n^m(\cos\theta)\, a^2 \sin\theta \,\mathrm{d}\theta \,\mathrm{d}\phi \end{aligned} \tag{B.5}$$

where Ω_i is the area of the patch associated with the condensation function φ^i, according to the definition of the condensation function in Eq. (29).

The integrals that appear in these expressions are solved numerically by separating the integrals. The integration over ϕ can be solved analytically, while the integration over θ is evaluated numerically using a global adaptative quadrature and default error tolerances.

Appendix B.2. Condensed pressure induced by a plane wave

In order to calculate $\boldsymbol{P}_{\mathbf{1+2}}$, the condensed pressure induced by an acoustic plane wave in the infinite water domain 1+2, we consider the expression of the pressure induced by the plane wave expanded in spherical harmonics given in Eq. (34). Then, using the definition of the scalar product

in spherical coordinates of Eq. (28), we project it on the condensation functions. Considering the weighted spherical harmonics as condensation functions, the i^{th} component of the vector $\boldsymbol{P_{1+2}}$ is given by:

$$P_{1+2,i} = \langle p_i, \psi_{\nu,\mu} \rangle = P_i \sum_{n=0}^{+\infty} (2n+1)\, i^n j_n\,(k_0 a) \sqrt{\frac{2\nu+1}{4\pi} \cdot \frac{(\nu-\mu)!}{(\nu+\mu)!}} \cdot \iint_{\Omega} P_n\,(\cos\theta)\, P_\nu^\mu\,(\cos\theta)\, \mathrm{e}^{-\mathrm{i}\mu\phi} a \sin\theta \,\mathrm{d}\theta \,\mathrm{d}\phi \tag{B.6}$$

where $\psi_{\nu,\mu}$ corresponds to the i^{th} condensation function, as defined in Eq. (26).

For the 2D gate functions as condensation functions, the i^{th} component of $\boldsymbol{P}_{\mathbf{1+2}}^{\boldsymbol{M_1}}$ is given by:

$$P_{1+2,i} = \left\langle p_i, \varphi^i \right\rangle = P_i \sum_{n=0}^{+\infty} (2n+1)\, i^n j_n\,(k_0 a)\, \frac{1}{\sqrt{\Omega_i}} \iint_{\Omega_i} P_n\,(\cos\theta)\, a^2 \sin\theta \,\mathrm{d}\theta \,\mathrm{d}\phi \tag{B.7}$$

where Ω_i is the area of the patch associated with the condensation function φ^i, according to the definition of the condensation function in Eq. (29).

References

[1] F. Firestone, The mobility method of computing the vibration of linear mechanical and acoustical systems: mechanical-electrical analogies, J. Appl. Phys. 9 (6) (1938) 373–387. doi:10.1063/1.1710432.

[2] S. Rubin, Transmission matrices for vibration and their relation to admittance and impedance, J. Eng. Ind. 86 (1) (1964) 9–21. doi:10.1115/1.3670463.

[3] G. O'Hara, Mechanical impedance and mobility concepts, J. Acoust. Soc. Am. 41 (5) (1967) 1180–1184. doi:10.1121/1.1910456.

[4] B. Petersson, J. Plunt, On effective mobilities in the prediction of structure-borne sound transmission between a source structure and a receiving structure, part II: Procedures for the estimation of mobilities, J. Sound Vib. 82 (4) (1982) 531–540. doi:10.1016/0022-460X(82)90406-0.

[5] B. Petersson, J. Plunt, On effective mobilities in the prediction of structure-borne sound transmission between a source structure and a receiving structure, part I: Theoretical background and basic experimental studies, J. Sound Vib. 82 (4) (1982) 517–529. doi:10.1016/0022-460X(82)90405-9.

[6] S. Kim, M. Brennan, A compact matrix formulation using the impedance and mobility approach for the analysis of structural-acoustic systems, J. Sound Vib. 223 (1) (1999) 97–113. doi:10.1006/jsvi.1998.2096.

[7] M. Ouisse, L. Maxit, C. Cacciolati, J.-L. Guyader, Patch transfer function as a tool to couple linear acoustic problems, J. Vib. Acoust. 127 (2005) pp. 458–466.

[8] G. Veronesi, C. Albert, E. Nijman, J. Rejlek, A. Bocquillet, Patch transfer function approach for analysis of coupled vibro-acoustic problems involving porous materials, in: SAE Technical Paper, 2014, pp. 2014–01–2092. doi:10.4271/2014-01-2092.

[9] J.-D. Chazot, J.-L. Guyader, Prediction of transmission loss of double panels with a patch-mobility method, J. Acoust. Soc. Am. 121 (1) (2007) 267–278. doi:10.1121/1.2395920.

[10] J.-D. Chazot, J.-L. Guyader, Transmission loss of double panels filled with porogranular materials, J. Acoust. Soc. Am. 126 (6) (2009) 3040–3048. doi:10.1121/1.3245033.

[11] L. Maxit, C. Yang, L. Cheng, J.-L. Guyader, Modeling of micro-perforated panels in a complex vibro-acoustic environment using patch transfer function approach, J. Acoust. Soc. Am. 131 (3) (2012) 2118–2130. doi:10.1121/1.3682055.

[12] X. Yu, L. Cheng, J.-L. Guyader, Modeling vibroacoustic systems involving cascade open cavities and micro-perforated panels, J. Acoust. Soc. Am. 136 (2) (2014) 659–670. doi:10.1121/1.4887442.

[13] X. Zhang, L. Cheng, Acoustic silencing in a flow duct with micro-perforated panel liners, Appl. Acoust. 167 (2020) 107382. doi:10.1016/j.apacoust.2020.107382.

[14] M. Aucejo, N. Totaro, J.-L. Guyader, Identification of source velocities on 3D structures in non-anechoic environments: Theoretical background and experimental validation of the inverse patch transfer functions method, J. Sound Vib. 329 (18) (2010) 3691–3708. doi:10.1016/j.jsv.2010.03.032.

[15] D. Vigoureux, N. Totaro, J. Lagneaux, J.-L. Guyader, Inverse patch transfer functions method as a tool for source field identification, J. Vib. Acoust. 137 (2) (2015) 021006. doi:10.1115/1.4029000.

[16] S. Forget, N. Totaro, J. Guyader, M. Schaeffer, Source fields reconstruction with 3D mapping by means of the virtual acoustic volume concept, J. Sound Vib. 381 (1) (2016) 48–64. doi:10.1016/j.jsv.2016.06.019.

[17] M. Aucejo, L. Maxit, N. Totaro, J.-L. Guyader, Convergence acceleration using the residual shape technique when solving structure–acoustic coupling with the Patch Transfer Functions method, Comput. Struct. 88 (11) (2010) 728–736. doi:10.1016/j.compstruc.2010.02.010.

[18] L. Maxit, M. Aucejo, J.-L. Guyader, Improving the Patch Transfer Function approach for fluid-structure modelling in heavy fluid, J. Vib. Acoust. 134 (5) (2012) 051011. doi:10.1115/1.4005838.

[19] V. Meyer, L. Maxit, J.-L. Guyader, T. Leissing, C. Audoly, A condensed transfer function method as a tool for solving vibroacoustic problems, Proceedings of the Institution of Mechanical Engineers, Part C: Journal of Mechanical Engineering Science 230 (6) (2016) 928–938. doi:10.1177/0954406215615627.

[20] V. Meyer, L. Maxit, J.-L. Guyader, T. Leissing, Prediction of the vibroacoustic behavior of a submerged shell with non-axisymmetric internal substructures by a condensed transfer function method, J. Sound Vib. 360 (2016) 260–276. doi:10.1016/j.jsv.2015.09.030.

[21] Z. Hu, L. Maxit, L. Cheng, Piecewise convergence behavior of the condensed transfer function approach for mid-to-high frequency modelling of a panel-cavity system, J. Sound Vib. 435 (2018) 119–134. doi:10.1016/j.jsv.2018.08.010.

[22] Z. Hu, L. Maxit, L. Cheng, Mid-to-high frequency piecewise modelling of an acoustic system with varying coupling strength, Mech. Syst. Signal Pr. 134 (2019) 106312. doi:10.1016/j.ymssp.2019.106312.

[23] E. A. Skelton, J. James, Acoustics of an anisotropic layered cylinder, J. Sound Vib. 161 (2) (1993) 251–264. doi:10.1006/jsvi.1993.1070.

[24] D. C. Ricks, H. Schmidt, A numerically stable global matrix method for cylindrically layered shells excited by ring forces, J. Acoust. Soc. Am. 95 (6) (1994) 3339–3349. doi:10.1121/1.409953.

[25] C. Dutrion, F. Simon, Acoustic scattering reduction using layers of elastic materials, J. Sound Vib. 388 (2017) 53–68. doi:10.1016/j.jsv.2016.10.034.

[26] M. Dana, L. Maxit, J. Bernard, Vibroacoustic response of an immersed stiffened multilayered shell excited by a plane wave, in: INTERNOISE 2018 - 47th International Congress on Noise Control Engineering, Chicago, United States, 2018.

[27] M. Dana, J. Bernard, L. Maxit, A spectral global matrix method for modelling the response of a fluid-loaded multilayered cylindrical shell excited by an acoustic plane wave, J. Acoust. Soc. Am. accepted for publication (2020).

[28] D. T. Soedel, W. Soedel, Synthesizing reduced systems by complex receptances, J. Sound Vib. 179 (5) (1995) 855 – 867. doi:https://doi.org/10.1006/jsvi.1995.0057.

[29] D. T. Huang, E. C. Ting, Vibration of plates with sub-structural deduction: a reverse receptance approach, J. Sound Vib. 271 (1-2) (2004) 177–207. doi:10.1016/S0022-460X(03)00368-7.

[30] D. T. Huang, A reverse receptance approach for analysis of vibration of grooved plates, Int. J. Mech. Sci. 53 (12) (2011) 1084–1102. doi:10.1016/j.ijmecsci.2011.09.003.

[31] D. T. Huang, Effects of constraint, circular cutout and in-plane loading on vibration of rectangular plates, Int. J. Mech. Sci. 68 (2013) 114–124. doi:10.1016/j.ijmecsci.2013.01.005.

[32] W. D'Ambrogio, A. Fregolent, Promises and pitfalls of decoupling procedures, in: 26th IMAC: Conference and Exposition on Structural Dynamics, Orlando, United States, 2008, p. 8.

[33] W. D'Ambrogio, A. Fregolent, The role of interface DoFs in decoupling of substructures based on the dual domain decomposition, Mech. Syst. Signal Pr. 24 (7) (2010) 2035–2048. doi:10.1016/j.ymssp.2010.05.007.

[34] S. Voormeeren, D. Rixen, A family of substructure decoupling techniques based on a dual assembly approach, Mech. Syst. Signal Pr. 27 (2012) 379–396. doi:10.1016/j.ymssp.2011.07.028.

[35] O. Tuysuz, Y. Altintas, Frequency domain updating of thin-walled workpiece dynamics using reduced order substructuring method in machining, J. Manuf. Sci. E-T. Asme 139 (7) (2017) 071013. doi:10.1115/1.4036124.

[36] M. Junger, D. Feit, Sound, structures and their interaction, MIT Press Cambridge, Second edition, 1986.

[37] R. J. Barton, K. B. Smith, H. T. Vincent, A characterization of the scattered acoustic intensity field in the resonance region for simple spheres, J. Acoust. Soc. Am. 129 (5) (2011) 2772–2784. doi:10.1121/1.3559689.

[38] D. Liu, H. Peters, S. Marburg, N. Kessissoglou, Surface contributions to scattered sound power using non-negative intensity, J. Acoust. Soc. Am. 140 (2) (2016) 1206–1217. doi:10.1121/1.4961200.

[39] G. S. Sharma, A. Skvortsov, I. MacGillivray, N. Kessissoglou, Sound transmission through a periodically voided soft elastic medium submerged in water, Wave Motion 70 (2017) 101–112. doi:10.1016/j.wavemoti.2016.10.006.

[40] G. S. Sharma, A. Skvortsov, I. MacGillivray, N. Kessissoglou, Sound absorption by rubber coatings with periodic voids and hard inclusions, Appl. Acoust. 143 (2019) 200–210. doi:10.1016/j.apacoust.2018.09.003.

[41] F. J. Fahy, Some applications of the reciprocity principle in experimental vibroacoustics, Acoust. Phys. 49 (2) (2003) 217–229. doi:10.1134/1.1560385.

[42] C. Marchetto, L. Maxit, O. Robin, A. Berry, Vibroacoustic response of panels under diffuse acoustic field excitation from sensitivity functions and reciprocity principles, J. Acoust. Soc. Am. 141 (6) (2017) 4508–4521. doi:10.1121/1.4985126.

[43] V. Meyer, L. Maxit, C. Audoly, A substructuring approach for modeling the acoustic scattering from stiffened submerged shells coupled to non-axisymmetric internal structures, J. Acoust. Soc. Am. 140 (3) (2016) 1609–1617. doi:10.1121/1.4962235.

[44] T. Valier-Brasier., Rayonnement acoustique [Acoustic radiation], Université Pierre et Marie Curie, 2017.